EarthArXiv Preprint

This manuscript is a preprint that has not yet undergone peer review.

Title:

Emerging climate–yield re-coupling in overexploited date palm oases:
satellite evidence from a 22-year temporal decoupling index in southern Tunisia

Authors:

Tarek Gasmi, Ramzi Guesmi, Slim Abdelbari, Soura Boulaares, Sajeda Albarghati

Date:

May 2026

Corresponding author: Tarek Gasmi (tarek.gasmi@manouba.tn)

Data and code: https://doi.org/10.5281/zenodo.20172850

Emerging climate–yield re-coupling in overexploited date palm oases: satellite evidence from a 22-year temporal decoupling index in southern Tunisia

Tarek Gasmi[a,*], Ramzi Guesmi[b], Slim Abdelbari[c], Soura Boulaares[d], Sajeda Albarghati[e]

[a] *University of Manouba, Tunisia*
[b] *University of Jendouba, Tunisia*
[c] *University of Sousse, Tunisia*
[d] *MUST University, Tunisia*
[e] *DataDoIt, Tunisia*

Abstract

Southern Tunisia's date palm oases have quadrupled production over two decades while extracting fossil groundwater at more than twice the sustainable rate, a trajectory whose consequences remain undetected by conventional monitoring. We analysed the 2002–2024 satellite, climate, and ground record across four governorates to test whether this irrigation buffer — the aquifer's capacity to absorb climate variability on behalf of the crop — is still intact or already degrading.

The buffer is still largely effective: no satellite or climate covariate carries a learnable signal about interannual yield anomalies, and every model we tested performs worse than a naive trend baseline. But the resource sustaining that buffer is disappearing. GRACE/GRACE-FO terrestrial water storage has declined by 16.6 cm since 2002, with the aquifer approximately stable through the mid-2000s and then declining at roughly 1 cm per year. And in Kébili, the governorate with the most overexploited aquifer (229 % of renewable resources), the buffer is already cracking: per-hectare yield has become progressively more sensitive to vapour pressure deficit over the study period

*Corresponding author.
Email address: tarek.gasmi@manouba.tn (Tarek Gasmi)

(HAC-corrected $p < 0.001$), a signal that strengthens after area normalisation ($\Delta|r| = +0.444$) and is robust to detrending method and placebo-feature tests, though it emerges from an exploratory scan and does not survive FDR correction in the full grid. Tozeur shows a similar pattern; Gafsa's signal is tentative.

In these oases, satellite monitoring detected the onset of buffer degradation years before any decline appeared in the production record, suggesting that the primary value of earth observation in aquifer-dependent agriculture lies in tracking buffer integrity rather than predicting yields.

Keywords: Date palm, Oasis agriculture, GRACE terrestrial water storage, Vapour pressure deficit, Temporal decoupling index, Aquifer overexploitation, Tunisia

---

1. Introduction

1.1. The oasis paradox and groundwater risk

Southern Tunisia's date palm oases present a contradiction that irrigation science is poorly equipped to resolve. Production has grown dramatically over the last two decades, with the four date-producing governorates of Tozeur, Kébili, Gafsa, and Gabès now accounting for essentially the entire national crop. Yet this growth rests on fossil water drawn from the shared deep aquifer system of the northern Sahara — the Continental Intercalaire and Complexe Terminal, together the Système Aquifère du Sahara Septentrional (SASS) — at rates that the Tunisian Court of Audit and the World Bank have both documented as structurally unsustainable (Mamou et al., 2006; Observatoire du Sahara et du Sahel (OSS), 2002; World Bank Group and Ministry of Agriculture, Tunisia, 2024; National Court of Audit of Tunisia, 2019; Kinzelbach et al., 2021; Besser et al., 2017). National audits now report deep-aquifer exploitation above 100 % of renewable resources nationally and above 200 % locally.

Kébili is the extreme case. Its post-1980 *nouvelles créations* scheme — deep-aquifer development permits opened to private capital — transformed the aquifer from a state-managed commons into a privately capitalised resource;

informal extraction has proliferated to the point where registered private wells have grown by roughly +185 % in fifteen years (World Bank Group and Ministry of Agriculture, Tunisia, 2024; Mekki et al., 2022). Production has risen in lockstep. On the surface, the system looks healthy: tonnages climb, yields per hectare climb, new plantations are established each year. Beneath the surface, the water table is falling at a rate that no steady-state irrigation regime can sustain.

Satellite gravity measurements have documented comparable groundwater depletion under irrigated agriculture in India (Rodell et al., 2009) and across the broader semi-arid belt (Famiglietti, 2014), and climate-change projections for Tunisian oases point to rising irrigation demand under future salinity and temperature scenarios (Haj-Amor et al., 2020). But the agricultural consequences of observed aquifer depletion — the question of whether and when overexploitation begins to affect the crop itself — have rarely been traced to production outcomes at operational scale.

The question this paper asks is therefore operational: can satellite observation detect when the trajectory of an overexploited oasis begins to cross an invisible threshold, before conventional monitoring metrics register a production decline?

1.2. Limits of satellite-based yield forecasting in irrigated systems

Satellite-based yield forecasting has matured into a standard tool of regional agricultural intelligence (Wang et al., 2023; Rashid et al., 2021; Kross et al., 2020; Brinkhoff and Robson, 2021; Sabo et al., 2025). Two assumptions are embedded in its design. The first is that year-to-year variation in crop outcomes is driven by year-to-year variation in weather. The second is that the effects of that variation are visible in the remotely sensed canopy. In rainfed cereal systems, both assumptions hold and the framework succeeds.

Neither holds in an irrigated desert oasis. The first fails because the design purpose of irrigation is to sever the link between weather and harvest; a system where forecasting works well is, by definition, a system where the irrigation

buffer has broken down. The second fails because *Phoenix dactylifera* is deep-rooted and perennial: its canopy greenness is buffered against short-term water stress by access to deep soil moisture, and alternate bearing (Alikhani-Koupaei et al., 2020) adds a biennial oscillation that further confounds interannual correlations. These constraints have been noted qualitatively in the irrigation-forecasting literature (Guillossou, 2025; Rigden et al., 2020; Jiang et al., 2020) and documented empirically for irrigated wheat (Tiedeman et al., 2022) and cloudy landscapes (Farhat et al., 2023), but no study has tested the prediction systematically on irrigated desert perennials.

The existing literature treats climate–yield decoupling through irrigation as a static property: a system is either irrigated and buffered, or rainfed and exposed (Guillossou, 2025; Rigden et al., 2020). This binary view offers no framework for detecting the transition point — the moment when overexploitation has degraded the aquifer sufficiently that the climate signal begins to penetrate the buffer. Vapour pressure deficit (VPD), the atmospheric drying power that drives stomatal closure in perennial crops (Grossiord et al., 2020; Lobell et al., 2014), is the variable most likely to reveal this transition: it quantifies the atmospheric water demand that the irrigation system must meet, and its effect on yield should be zero in a fully buffered system but increasingly negative as the buffer thins.

1.3. Objectives and contributions

This paper asks whether satellite earth observation can detect the onset of irrigation-buffer degradation in aquifer-dependent oases. We address this through three linked analyses. First, we test whether standard satellite-and-machine-learning yield forecasting works in irrigated date palm systems — and demonstrate that it does not, for physically informative reasons. Second, we quantify the groundwater depletion financing the observed production growth, using GRACE/GRACE-FO terrestrial water storage reconciled with ground-based aquifer accounting. Third, we introduce a temporal decoupling index that tracks how the sensitivity of per-hectare yield to atmospheric water demand

evolves over time, and we test whether its signal survives area normalisation — a condition without which the result could reflect expanding plantation area rather than genuine vulnerability.

The narrative is three-act: satellite-based forecasting fails because the irrigation buffer suppresses the climate signal; GRACE reveals that the resource sustaining that buffer is in steep decline; and the decoupling index detects where the buffer is already beginning to thin. Together, these findings reframe the role of satellite monitoring in aquifer-dependent irrigated systems: from yield prediction to buffer-integrity tracking.

2. Study area and data

2.1. Study region

The study covers the four southern Tunisian governorates that together produce essentially the entire national date crop (Figure 1). Tozeur and Kébili flank the Chott el Jerid salt depression and host the historical continental oases, irrigated primarily from the deep aquifers of the SASS. Gafsa sits to the north at the transition to the phosphate-mining belt, with mixed shallow and deep aquifer use. Gabès is the coastal governorate on the Gulf of Gabès, with mixed saline-shallow and freshwater-deep systems (Kharroubi et al., 2014).

The four governorates span a clear institutional and hydrological gradient. Tozeur is the oldest and most regulated system. Its Groupements de Développement Agricole (GDA) framework manages withdrawals within established perimeters, its deep-aquifer exploitation sits at 68–71 % of renewable resources, and its oasis area has expanded modestly. Kébili represents the opposite institutional regime. The *nouvelles créations* scheme described in §1.1 opened the deep aquifer to private capital; informal extraction has since proliferated, with registered private wells rising from approximately 3,700 in 2008 to more than 10,600 in 2023 (CRDA anchor points; the 2008 figure is from the World Bank and Ministry of Agriculture (2024) national investigations report (World Bank Group and Ministry of Agriculture, Tunisia, 2024)). Deep-aquifer ex-

ploitation in Kébili has reached 229 %. Gafsa and Gabès exceed 100 % on their shallow aquifers (163 % and 115 % respectively).

The governorates also differ in climate exposure. Across the four, mean annual precipitation (ERA5-Land, 2002–2024) rises from approximately 85 mm in Kébili and 95 mm in Tozeur to 140 mm in Gafsa and 200 mm in Gabès.

Study-area production has roughly tripled over 2002–2024, dominated by Kébili, which accounts for approximately 70 % of the four-governorate total. The growth trajectory and its decomposition into area expansion and yield improvement are quantified in §4.

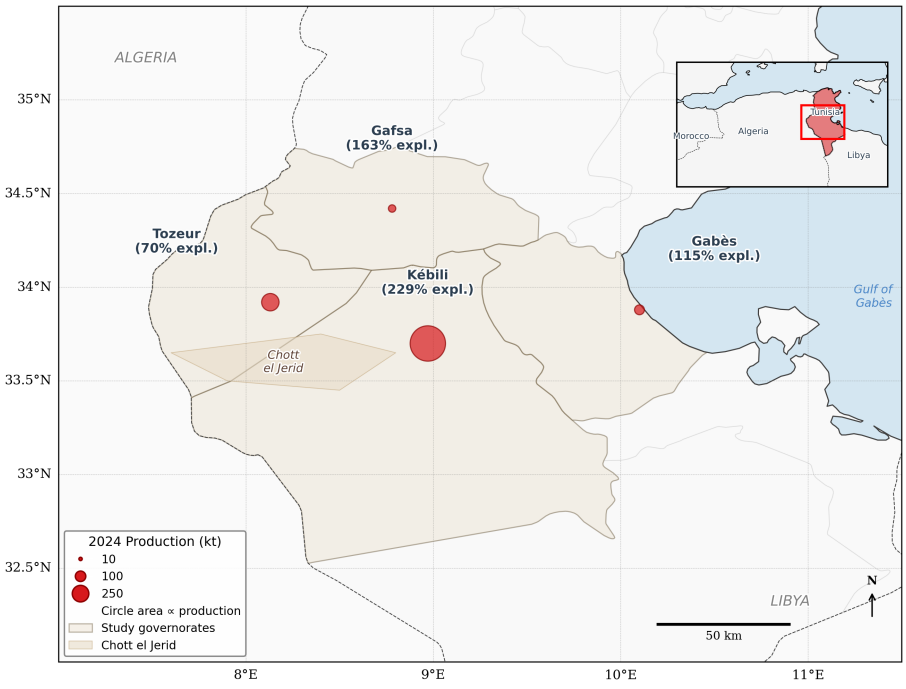

Figure 1: Study area in southern Tunisia. The four date-palm-producing governorates included in the analysis are shaded beige; red circles indicate 2024 date production, with circle area proportional to production (ONAGRI). Percentages in governorate labels are aquifer exploitation rates relative to renewable resources from CRDA bulletins and national audits — these refer to the deep aquifer in Kébili and Tozeur and to the shallow aquifer in Gafsa and Gabès. The Chott el Jerid salt depression is shown for geographic reference; the inset locates Tunisia within northern Africa. Administrative boundaries from FAO GAUL.

2.2. Datasets

The analysis combines satellite earth observation, atmospheric reanalysis, ground-based aquifer accounting, and agronomic production records. The satellite component provides vegetation state, land-surface temperature, precipitation and terrestrial water storage; the reanalysis component provides the atmospheric variables (temperature, dewpoint, wind, radiation) needed to derive VPD and reference evapotranspiration; the ground component provides production tonnages and aquifer bulletins. Table 1 summarises the main sources. Full product version identifiers are listed in the Supplementary Material.

ONAGRI production records are the official national series for date tonnage at governorate level. As with most governorate-level agricultural statistics in the MENA region, the series may include carried-forward estimates in years where fresh measurement was unavailable; data-quality implications are discussed in §5.4.

Two satellite products were excluded from the main analysis for insufficient coverage in the study area. MODIS evapotranspiration (MOD16A2) was excluded because valid-pixel coverage was insufficient in this hyper-arid landscape (Aguilar et al., 2018; Mu et al., 2011); a Hargreaves-style reference ET proxy is used instead (§3.1; Supplementary Text S2). Sentinel-2 surface reflectance was excluded from the annual modelling set because its coverage begins only in 2015, leaving too short a record for two-period and rolling-window analyses across 2002–2024; it is retained in a monthly companion dataset for intra-season applications.

GRACE/GRACE-FO terrestrial water storage anomalies were obtained from NASA PO.DAAC as monthly mascon solutions referenced to the 2004–2009 baseline; the disaggregation, gap-filling, and trend-analysis methodology is described in §3.2.

2.3. Oasis area and yield per hectare

Converting tonnages to yields per hectare requires a time-resolved estimate of palm area in each governorate. We use two complementary methods. For

Table 1: Principal data sources. Product version strings and access identifiers are listed in the Supplementary Material.

Product	Resolution	Period	Variables used
MODIS NDVI	1 km	2002–2024 (16-day)	Canopy vegetation index
MODIS land surface temperature	1 km	2002–2024 (8-day)	Day/night LST
ERA5-Land reanalysis	9 km	2002–2024 (monthly)	Temperature, dewpoint, radiation, wind
CHIRPS precipitation	5 km	2002–2024 (daily)	Precipitation totals, rain days
GRACE / GRACE-FO mascon	$\sim 3^{\circ}$	2002–2024 (monthly)	Terrestrial water storage anomaly
SRTM, SoilGrids	30–250 m	static	Elevation, soil texture
ONAGRI production records	governorate	2002–2024 (annual)	Date-palm tonnages
CRDA aquifer bulletins	gov. $\times$ aquifer	2020–2024	Extraction rates, well counts
Persistent-NDVI oasis area	governorate	2002–2024 (annual)	Palm footprint

the continental-oasis zones of Tozeur and Kébili, the dense-vegetation footprint at Chott margins is effectively pure palm, and we estimate annual area from a persistent-NDVI threshold applied across 2002–2024. For Gabès and Gafsa, the NDVI-persistent footprint includes substantial non-palm irrigated vegetation (olive, horticulture, coastal greenhouse production); here a supervised Random Forest classifier trained on Sentinel-2 reflectance and photo-interpreted training polygons provides a 2024 palm-fraction correction of 0.096 (Gabès) and 0.040 (Gafsa). The yield-per-hectare computation and its equation are presented in §3.4. The resulting governorate means of 5.7–5.8 $\mathrm{t\,ha^{-1}}$ are consistent with agronomic references for the Deglet Nour cultivar (Tiba et al., 2025; Belloumi and Matoussi, 2006). Classification accuracy and methodological details for the palm-fraction correction are reported in Supplementary Text S4, and a CRDA cross-check of the persistent-NDVI area product is reported in Supplementary Table S5.

The 2024 palm-fraction correction for Gabès and Gafsa is a snapshot; projecting it backwards across 22 years assumes the non-palm fraction of the oasis footprint has been stable, which is unverifiable. For this reason, the yield-per-hectare analysis reported below is restricted to Tozeur and Kébili, where the palm fraction is effectively 1.0 by construction and the normalisation is unambiguous. Gabès and Gafsa are retained for the production-anomaly analysis only.

3. Methods

The analytical framework proceeds in three stages that mirror the paper's findings. First, we test whether satellite-based yield forecasting works in these oases (§3.1), a question whose answer determines whether climate signals propagate into production at all. Second, we quantify the groundwater depletion that sustains the irrigation buffer (§3.2), establishing the resource trajectory. Third, we ask whether the buffer's effectiveness is changing over time, using a temporal decoupling index (§3.3) validated by area normalisation (§3.4). Each

stage informs the next: the forecasting failure measures the buffer's current strength; the GRACE decline reveals why that strength is finite; the decoupling index detects where it is already weakening.

3.1. Yield anomaly definition and forecasting test

Raw production is dominated by the cross-governorate scale contrast (Kébili produces roughly ten times more than Gafsa), so any model fitted on tonnes achieves a high R^2 by learning the governorate identity rather than interannual variation (Wang et al., 2023). We therefore target the production anomaly, defined as the percent deviation from a per-governorate linear trend:

$$a_{g,t} = 100 \cdot \frac{Y_{g,t} - \hat{Y}_{g,t}}{\hat{Y}_{g,t}} \tag{1}$$

where $\hat{Y}_{g,t}$ is the fitted value from ordinary-least-squares regression of production Y on year t over 2002–2024. Linear detrending is parameter-free and avoids the future-information problem inherent in centred rolling windows; alternative detrending definitions (rolling-window, trailing-window, first-differencing, quadratic) are reported as sensitivity analyses in Supplementary Table S2. The same anomaly definition is applied to yield per hectare.

The predictor set comprises annual features derived from the monthly satellite and reanalysis products: vegetation indices (MODIS NDVI), land-surface temperature, growing degree days (GDD above 18 °C), vapour pressure deficit during the fruit-development window, precipitation totals and rain days (CHIRPS), diurnal temperature range, wind speed, and a Hargreaves-style reference evapotranspiration proxy (Supplementary Text S2). Features were aggregated over three phenological windows relevant to date palm: pollination (March–April), fruit development (May–August), and harvest (September–November). After removing redundant predictors (pairwise $|r| > 0.95$; the pairwise correlation structure of the predictor set is shown in Supplementary Figure S2), the full set contains 111 features; a sparse 12-feature subset retaining only agronomically interpretable variables was also tested. Full feature definitions and the sparse-set composition are in Supplementary Text S3.

Three model families were fitted under leave-one-year-out cross-validation on 2002–2020, with a held-out test on 2021–2024: Ridge regression (regularised linear), Random Forest (non-linear interactions), and XGBoost (gradient-boosted ensemble). Hyperparameters are in Supplementary Table S1. Two baselines frame the comparison: a naive zero-anomaly baseline ($R^2 = 0$ by construction, the reference) and a persistence baseline that predicts this year's anomaly from last year's. Because *Phoenix dactylifera* exhibits alternate bearing, the within-governorate lag-1 anomaly correlation is strongly negative (approximately -0.53), and the persistence baseline is expected to underperform the naive baseline (Alikhani-Koupaei et al., 2020).

3.2. GRACE terrestrial water storage

At the JPL Mascon native resolution of approximately 3°, GRACE integrates the study region as a single regional signal; the four-governorate footprint sits within one to two mascons. We disaggregate this pooled signal to governorate level by weighting each governorate's contribution by its share of CRDA-documented extraction volumes:

$$\mathrm{TWS}_g(t) = \mathrm{TWS}_{\mathrm{regional}}(t) \cdot \frac{V_g}{\sum_{g'} V_{g'}} \tag{2}$$

where V_g is the mean annual extraction volume for governorate g from CRDA bulletins (Kébili 56.2 %, Tozeur 21.3 %, Gabès 16.9 %, Gafsa 5.6 %; 2020–2024 means). This is a pumping-share attribution: it assumes each governorate's contribution to the regional TWS decline is proportional to its share of documented extraction. It is not a spatial downscaling; it does not resolve intra-governorate aquifer structure. The approach is appropriate when the dominant driver of TWS change is anthropogenic extraction rather than spatially variable precipitation — a condition supported by the water-balance estimate in §4.2 and consistent with the GRACE groundwater methodology of Rodell et al. (2009) and Famiglietti (2014).

The CRDA extraction weights are derived from the 2020–2024 bulletins (the earliest with complete four-governorate coverage) and are projected backward

under a proportional-stability assumption: we assume the relative shares of extraction across governorates have remained approximately constant, even as absolute volumes have grown. This assumption is unverifiable before 2020 because earlier bulletins are incomplete, and it constitutes a limitation discussed in §5.4.

The 11-month GRACE/GRACE-FO mission-transition gap (June 2017–May 2018) is filled by linear interpolation, consistent with the continuity practice of Landerer et al. (2020). Annual values are calendar-year means of the monthly series.

To identify whether the depletion rate has changed over the study period, we fit a piecewise linear model:

$$\mathrm{TWS}(t) = \begin{cases} \alpha_1 + \beta_1\, t & \text{if } t \le t^*, \\ \alpha_2 + \beta_2\, t & \text{if } t > t^*, \end{cases} \tag{3}$$

where the break year t^* is identified by a sup-Wald (Bai–Perron) scan across candidate breaks in 2005–2020, selecting the break that minimises the pooled residual sum of squares. The scan is run under both independent-segment and continuous-piecewise specifications. The data-driven break is reported with its 95 % confidence interval; sensitivity to break-year choice in the ±2-year neighbourhood is also reported.

3.3. Temporal decoupling index

The decoupling index operationalises the intuition that a thinning irrigation buffer restores a correlation between climate and yield that had previously been suppressed. For a given governorate g, climate variable X (here, fruit-development-window VPD), and yield target Y (production anomaly or yield-per-hectare anomaly), we compute the Pearson correlation within a centred rolling window of width $w = 10$ years:

$$r_g(\tau) = \mathrm{Corr}\big(X_{g,t},\, Y_{g,t}\big) \quad \text{for } t \in \big[\tau - w/2,\ \tau + w/2\big], \tag{4}$$

with window centres τ spanning 2007–2019 for the 2002–2024 record (14 centres). We track the absolute value $|r_g(\tau)|$ rather than the signed correlation,

because re-coupling can manifest as either a positive or negative association depending on the climate variable and mechanism. A value of $|r|$ near zero indicates full decoupling: the irrigation buffer absorbs the climate signal. A rising $|r|$ indicates re-coupling: the climate signal is penetrating the buffer.

The temporal decoupling index is the slope of this trajectory:

$$\beta_g = \frac{\mathrm{d}\,|r_g(\tau)|}{\mathrm{d}\,\tau}, \tag{5}$$

estimated by OLS regression of $|r_g|$ on τ across the window centres. The sign of β has a direct physical interpretation: $\beta > 0$ indicates re-coupling (the buffer is thinning and climate variability increasingly affects yield); $\beta < 0$ indicates deepening decoupling (the buffer is strengthening); $\beta \approx 0$ indicates a stable coupling state.

A descriptive complement is the two-period contrast $\Delta|r| = |r_{\text{late}}| - |r_{\text{early}}|$, computed by splitting the record at 2012 into an early period (2002–2012) and a late period (2013–2024). This captures the same phenomenon at lower resolution and is easier to visualise than the rolling trend.

The computational machinery — rolling absolute correlation followed by a linear trend in the window centre — is standard; the contribution is the interpretive framework that connects the trend direction to irrigation-buffer degradation, and its operational application to fossil-aquifer-dependent agriculture. The index is dimensionless, requires only two time series (one climate, one yield), and is directly applicable to any irrigated system with a sub-national annual yield record.

Because adjacent rolling windows share $w - 1$ of w underlying years, the residuals of the $|r|$-on-τ regression are positively autocorrelated. We report the slope with Newey–West heteroskedasticity- and autocorrelation-consistent (HAC) standard errors using a Bartlett kernel at bandwidth $L = w - 1 = 9$, which reduces the effective degrees of freedom to approximately 12. The hypothesis test is one-sided:

$$H_0 : \beta_g \leq 0 \text{ (buffer stable or strengthening)} \quad \text{vs.} \quad H_1 : \beta_g > 0 \text{ (buffer thinning).} \tag{6}$$

VPD during the fruit-development window (May–August) is the focal climate variable. It is derived from ERA5-Land 2 m temperature and dewpoint via the Tetens formulation:

$$\mathrm{VPD} = e_s(T) - e_s(T_d), \qquad e_s(T) = 0.6108 \cdot \exp\left(\frac{17.27\,T}{T + 237.3}\right). \tag{7}$$

VPD is the appropriate focal variable on physiological grounds: it is the atmospheric water-demand scalar that drives stomatal closure in perennial crops (Grossiord et al., 2020; Hao et al., 2025; Rigden et al., 2020), and the thinning-buffer hypothesis specifically predicts a VPD-sensitivity recovery as subsurface water retreats. The choice of VPD was informed by an exploratory comparison of four candidate climate variables (VPD, precipitation, growing degree days, NDVI), and the resulting exploratory-testing context is carried through the analysis: the VPD result is interpreted as a convergent monitoring signal rather than a stand-alone hypothesis test, and Benjamini–Hochberg-corrected q-values for the full 32-cell grid (4 governorates × 4 features × 2 targets) are reported in Supplementary Table S4.

Robustness is assessed through break-year sensitivity (6 alternative breaks), detrending-method sensitivity (5 methods including quadratic), and a seven-feature placebo panel; full details including bootstrap methodology are in Supplementary Text S1 and Tables S2–S4.

3.4. Area normalisation test

A decoupling signal observed on raw production could be a spatial-composition artefact: new plantations established at the expanding margins of an oasis might inflate the climate–yield correlation even if the underlying physiological buffer were unchanged. Dividing production by palm area isolates the per-hectare signal:

$$y_{g,t} = \frac{P_{g,t}}{A_{g,t} \cdot f_g}, \tag{8}$$

where P is production (tonnes), A is satellite-derived oasis area (hectares), and f is the palm fraction (1.0 for Kébili and Tozeur, 0.096 for Gabès, 0.040 for Gafsa). If the decoupling signal survives this normalisation in the two governorates

where the palm fraction is unambiguous, it is less likely to be explained solely by area expansion and is consistent with a real change in the climate–yield relationship. The yield-per-hectare analysis is restricted to Tozeur and Kébili for the reasons set out in Section 2.3.

4. Results

4.1. Satellite-based yield forecasting fails in irrigated oases

Table 2 reports the model comparison on held-out 2021–2024 data. On the anomaly target — the interannual variation the model is actually attempting to explain — all three learned models return negative anomaly R^2 on the held-out test (Table 2), performing worse than the naive zero-anomaly baseline. The naive baseline returns $R^2 = 0$ by construction. Predicted-versus-actual scatter is shown in Figure 2: on the anomaly scale (panel b), predictions collapse toward the baseline rather than tracking the realised year-to-year deviations.

Table 2: Comparison of learned models and baselines on the held-out 2021–2024 test. Tonnes-scale R^2 exceeds 0.99 for every row and is scale-dominated (see text); it is omitted. pp = percentage points; MAPE = mean absolute percentage error (tonnes scale).

Model	Split	MAE (pp)	RMSE (pp)	R^2 (anom.)	MAPE (%)
Naive zero-anomaly baseline	Test	σ	σ	0.000	≈ 4.2
Persistence (lag-1 anomaly)	Test	8.39	10.52	−3.523	8.42
Simple OLS (yield-anom ∼ VPD)	Test	4.29	5.03	−0.032	—
Ridge	Test	4.47	5.19	−0.102	4.45
Random Forest	Test	4.86	5.63	−0.294	4.83
XGBoost	Test	5.34	5.86	−0.407	5.29

The persistence baseline performs notably worse than the naive baseline ($R^2 = -3.52$), consistent with the biennial alternate-bearing cycle in date palm (§5.1). A simple ordinary-least-squares regression of yield anomaly on fruit-development VPD alone — the smallest possible climate-yield model — also fails on the same held-out test ($R^2 = -0.03$), confirming that the negative

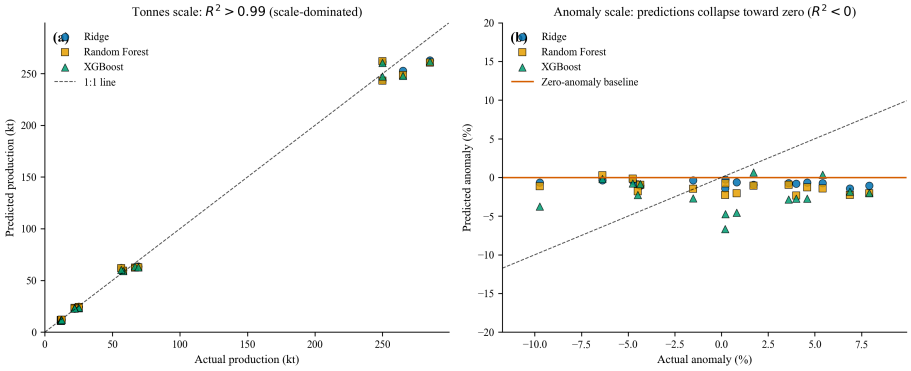

Figure 2: Predicted versus actual for Ridge, Random Forest and XGBoost on the 2021–2024 held-out test. (a) Tonnes scale: predictions cluster near the 1:1 line and yield $R^2 > 0.99$, but this is governed by the cross-governorate level contrast and not by anomaly skill. (b) Anomaly scale: predictions collapse toward the zero-anomaly reference (red line), yielding negative out-of-sample R^2.

result is not an artefact of model complexity or feature curation. We emphasise that this result applies to satellite and climate covariates only. We did not test pure autoregressive models that exploit production history (§5.1); such models might recover short-term predictability from the alternate-bearing signal, but that would confirm rather than contradict the decoupling hypothesis presented in this paper.

Tonnes-scale R^2 exceeds 0.99 for every model but is scale-dominated (§5.1). SHAP feature attributions for the XGBoost model show no stable feature ranking across leave-one-year-out folds (Supplementary Figure S1), consistent with the absence of a learnable anomaly signal in the satellite/climate covariates.

4.2. GRACE reveals accelerating groundwater depletion

The study-area-mean GRACE terrestrial water storage anomaly falls monotonically from +0.32 cm (2002–2005 mean) to −16.26 cm (2020–2024 mean), a net loss of 16.6 cm of liquid-water equivalent over 22 years (Figure 3). The deepest single-year value is −18.04 cm in 2024.

The depletion rate is not constant. A sup-Wald scan over candidate break

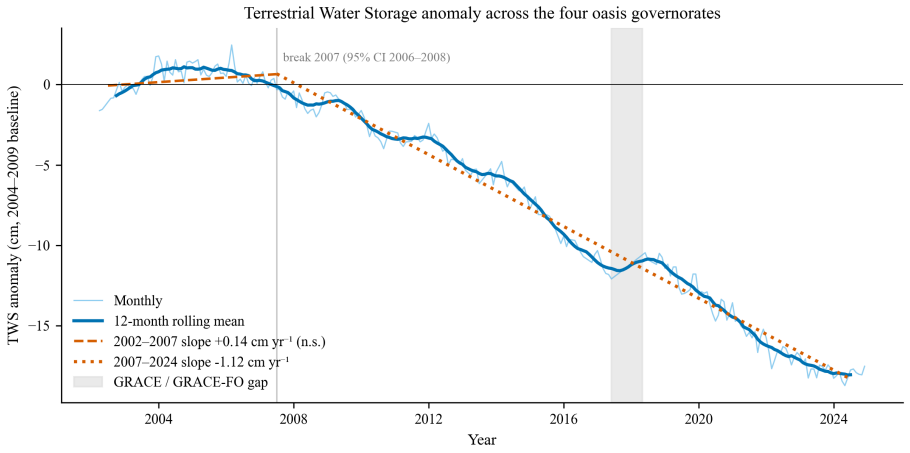

Figure 3: GRACE and GRACE-FO terrestrial water storage anomaly over the four-governorate footprint, 2002–2024. Monthly values (light), 12-month rolling mean (heavy), and piecewise linear trends with break year identified by the sup-Wald scan (2007; 95 % CI 2006–2008). The GRACE/GRACE-FO mission-transition gap is shaded.

years identifies a structural break at **2007** (95 % confidence interval 2006–2008) at which the regression's residual sum of squares is minimised. A piecewise linear fit with the break at 2007 returns a near-zero slope of $+0.14\,\mathrm{cm\,yr^{-1}}$ (2002–2007, $R^2 = 0.14$, $p = 0.47$) followed by $-1.12\,\mathrm{cm\,yr^{-1}}$ (2007–2024, $R^2 = 0.99$, $p < 10^{-15}$): the storage record is approximately stable through the mid-2000s and then declines monotonically at a rate of more than one centimetre per year for the remainder of the record. Anchoring the break instead at 2012 (an earlier visual choice) returns a still-significant rate change from -0.43 to $-1.19\,\mathrm{cm\,yr^{-1}}$, with weaker pre-break fit ($R^2 = 0.67$); we report this for continuity with previous SASS-region work. The single-period 2002–2024 fit explains 95 % of the interannual variance, confirming that the dominant signal is a secular decline rather than year-to-year noise. A first-order water-balance estimate — given a four-governorate footprint of approximately 42,000 $\mathrm{km^2}$, mean annual precipitation of 120 mm, and arid-zone recharge fractions of 1–10 % — places the maximum climatic contribution to the observed loss at roughly 5 cm. The remaining 12 cm or more is anthropogenic.

Ground evidence corroborates this picture. The aquifer exploitation rates and well-proliferation trajectory documented in §2.1 — with Kébili's deep aquifer at 229 % of renewable resources and registered private wells nearly tripling between 2008 and 2023 — are quantitatively consistent with the magnitude of the observed GRACE decline. Per-governorate scatter of TWS against yield-anomaly is shown in Supplementary Figure S5.

4.3. VPD–yield coupling rises robustly in Kébili and Tozeur, tentatively in Gafsa

Production growth in the study area has been dominated by Kébili, where the 2020–2024 period mean exceeds the 2002–2006 mean by a factor of 4.10. This growth decomposes approximately into a 1.87× area expansion and a 2.19× yield-per-hectare increase, the latter enabled by expanded pumping capacity. Across all four governorates, fruit-development-window VPD has risen by 12–15 % between period means, consistent with the continental-scale atmospheric drying documented by Grossiord et al. (2020). The question the decoupling analysis addresses is whether this rising atmospheric demand is beginning to penetrate the irrigation buffer.

Under linear detrending, the two-period $\Delta|r|$ between fruit-development-window VPD and production anomaly is positive in three of four governorates (Table 3). On the area-normalised yield-per-hectare anomaly in Tozeur and Kébili — the two governorates where the palm fraction is unambiguous — the values are +0.604 (Tozeur) and +0.444 (Kébili). Figure 4 presents the scatter for both governorates on both targets.

The rolling 10-year absolute correlation (Figure 5) shows a consistent rise in three of the four governorates: Tozeur at $+0.046\,\mathrm{yr}^{-1}$, Kébili at $+0.031\,\mathrm{yr}^{-1}$, and Gafsa at $+0.045\,\mathrm{yr}^{-1}$. Under HAC-corrected inference, all three slopes show a consistent positive trend ($p < 0.05$, with Kébili and Gafsa at $p < 0.001$; effective $df \approx 12$, and interpretation should account for the strong temporal dependence among overlapping windows). Gabès is not significant ($+0.011\,\mathrm{yr}^{-1}$, $p = 0.30$). Kébili's absolute correlation rises from near zero in the earliest windows to above 0.5 in recent windows. We treat the Kébili and Tozeur slopes

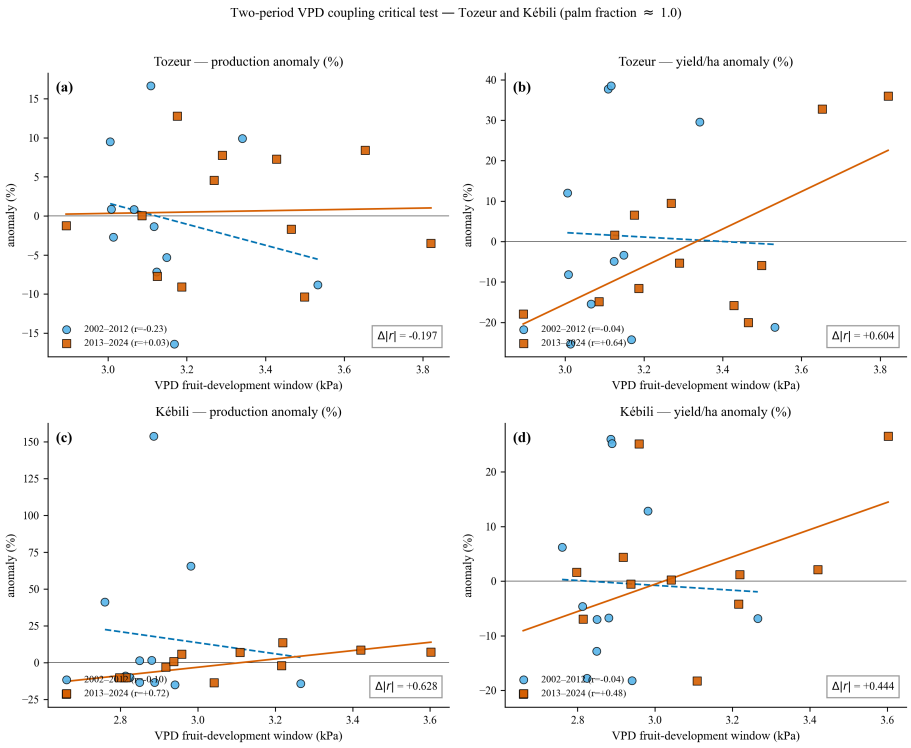

Figure 4: Two-period VPD coupling for Tozeur and Kébili under linear detrending. Scatter of production anomaly (left column) or yield-per-hectare anomaly (right column) against fruit-development-window VPD, split at 2012. 2002–2012 (open circles) and 2013–2024 (filled squares) with per-period regression lines; $\Delta|r|$ annotations show the coupling shift.

as robust because they survive every sensitivity test, including quadratic detrending of yield (next paragraph; Supplementary Table S2). Gafsa's slope is significant but its two-period contrast collapses under quadratic detrending, so the Gafsa result is reported tentatively pending replication on a longer record.

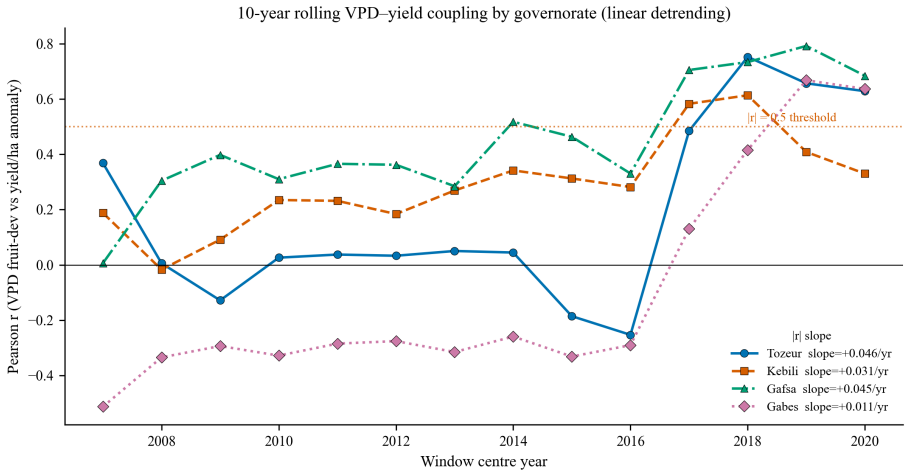

Figure 5: Rolling 10-year absolute correlation between fruit-development-window VPD and yield-per-hectare anomaly by governorate. Three of four governorates (Tozeur, Kébili, Gafsa) show a positive trend under HAC-corrected inference; Gabès is essentially flat. The Kébili and Tozeur trends survive quadratic detrending of yield; Gafsa's two-period contrast does not (Supplementary Table S2), so the Gafsa rolling slope is reported tentatively.

The finding is robust to break-year choice (positive $\Delta|r|$ at all tested breaks from 2010 to 2015), to three of four detrending methods (the exception being a trailing-only rolling window, which suffers from initialisation noise in the first few years of the series), and to a seven-feature placebo panel in which VPD's $\Delta|r|$ exceeds all climatically neutral alternatives. The signal also survives quadratic detrending of the yield series (Kébili $\Delta|r| = +0.413$, Tozeur $+0.425$, Supplementary Table S2), ruling out the possibility that residual nonlinear co-trends between VPD and yield drive the result; Gafsa's two-period $\Delta|r|$ collapses under quadratic detrending of yield, although its rolling-window slope remains significant. The HAC-corrected rolling slope for Kébili (14 window centres, effective $df \approx 12$ after Newey–West correction with Bartlett kernel at lag 9) shows

$p < 0.001$. The two-period bootstrap confidence interval around the Kébili point estimate is wide, reflecting the roughly twelve observations per period, but the rolling-window trend is the primary inferential test. Full robustness details are in Supplementary Tables S2–S4. The pooled four-governorate rolling correlation is shown in Supplementary Figure S3, and the per-governorate rolling $|r|$ time-series view that complements the rolling slopes in Figure 5 is in Supplementary Figure S4.

Area normalisation strengthens rather than weakens the finding. For Kébili, $\Delta|r|$ rises from approximately +0.29 on production to +0.444 on yield per hectare. For Tozeur, a re-coupling signal that is absent at the tonnes level ($\Delta|r| = -0.20$) emerges strongly at the yield-per-hectare level ($\Delta|r| = +0.604$), a signal hidden by Tozeur's institutionally smoothed production trajectory. The surviving and strengthened signals indicate that the coupling shift is not adequately explained by spatial composition due to expanding plantation area. Figure 6 assembles four independent lines of evidence for Kébili — production trajectory, well proliferation, GRACE depletion, and VPD–yield coupling — that triangulate on a single process: the irrigation buffer is thinning while aggregate production continues to rise.

4.4. Interpretation of the positive coupling sign

The late-period correlation between VPD and yield per hectare in Kébili is positive ($r = +0.48$), not negative, and this sign merits explicit comment before the Discussion to avoid misreading. Agronomic intuition from rainfed crops treats high VPD as a stressor that closes stomata and reduces carbon assimilation (Grossiord et al., 2020; Lobell et al., 2014). But Deglet-Nour is a heat-demanding cultivar whose fruit quality and sugar accumulation depend on sustained high temperatures during the late-ripening (Tamar) stage from July to October (Faci and Benziouche, 2021), with applied-water requirements that a well-functioning deep-aquifer irrigation system is designed to satisfy (Tiba et al., 2025). High-VPD years in southern Tunisia are simultaneously high-temperature, high-radiation years that drive thermal accumulation beneficial

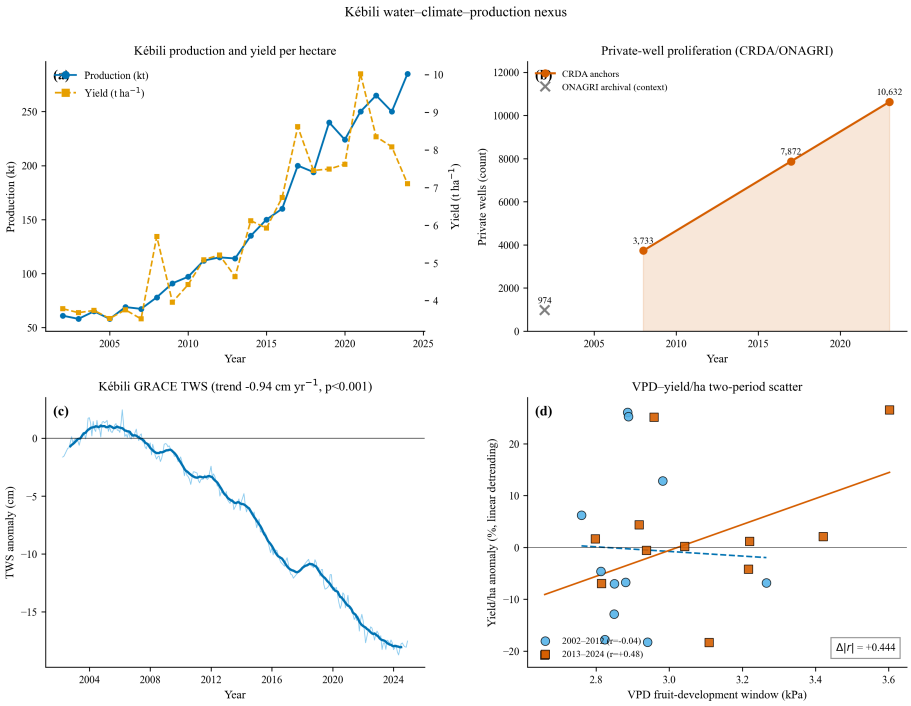

Figure 6: Kébili water–climate–production nexus. (a) Production and yield-per-hectare trajectory. (b) CRDA-registered private-well count. (c) GRACE terrestrial water storage with linear trend (Kébili extraction-weighted share). (d) Two-period scatter of linear-detrended yield-per-hectare anomaly against fruit-development-window VPD; 2002–2012 (open circles) and 2013–2024 (filled squares).

to yield. In a fully buffered regime, the water-demand cost of high VPD is absorbed by pumping while the thermal-benefit component is fully captured: the observed correlation is zero or weakly positive. As the buffer thins, the water-demand cost begins to offset the thermal benefit. That the late-period r remains positive rather than negative indicates Kébili has not yet crossed the point where water limitation dominates thermal benefit; it is in a transition zone where VPD has started to matter but has not yet become net-harmful. A future sign flip from positive to negative would mark that threshold crossing.

To distinguish water-demand sensitivity from thermal-accumulation sensitivity, we computed partial correlations between VPD and yield-per-hectare anomaly in the late period (2013–2024) controlling for confounding thermal variables. After removing the variance explained by mean fruit-development-window air temperature, Kébili's VPD–yield partial correlation rises to $r_{\text{partial}} = +0.69$ ($p = 0.014$); after removing both annual GDD_{18} and mean temperature jointly, $r_{\text{partial}} = +0.68$ ($p = 0.015$). For comparison, the early-period (2002–2012) partial correlations under the same controls are -0.10 and $+0.10$ respectively, both indistinguishable from zero. The strengthening of the VPD–yield association after thermal-variable control — not its attenuation — supports the interpretation that VPD is carrying water-demand information beyond what temperature alone explains. For Tozeur the partial correlations attenuate more (joint-control $r_{\text{partial}} = +0.39$, $p = 0.21$), consistent with a weaker but still positive water-demand signal in the more institutionally regulated governorate. These partial correlations are based on approximately 12 late-period observations and should be interpreted as supporting diagnostics consistent with the water-demand hypothesis, not as confirmatory evidence.

Table 3 consolidates the headline numerical evidence across the three findings.

Table 3: Study-level evidence summary. Gafsa is reported tentatively because its two-period $\Delta|r|$ contrast does not survive quadratic detrending of the yield series (Supplementary Table S2).

Indicator	Value	Governorate
GRACE TWS change (2002–05 → 2020–24)	-16.6 cm l.w.e.	pooled
TWS rate 2002–2007 (data-driven break)	$+0.14\,\mathrm{cm\,yr^{-1}}$ (n.s.)	pooled
TWS rate 2007–2024	$-1.12\,\mathrm{cm\,yr^{-1}}$ ($p < 0.001$)	pooled
Best learned model R^2 (anomaly, test)	-0.10 (Ridge)	pooled
Naive baseline R^2 (anomaly)	0.00 (reference)	pooled
Deep-aquifer exploitation	229 % (2022–23)	Kébili
Private wells, 2008 → 2023	3,733 → 10,632 (+185 %)	Kébili
$\Delta\|r\|$ VPD–yield/ha (two-period, linear)	+0.444	Kébili
$\Delta\|r\|$ VPD–yield/ha (two-period, linear)	+0.604	Tozeur
Rolling $\|r\|$ slope (10-yr, HAC)	$+0.031\,\mathrm{yr^{-1}}$, $p < 0.001$	Kébili
Rolling $\|r\|$ slope (10-yr, HAC)	$+0.046\,\mathrm{yr^{-1}}$, $p = 0.011$	Tozeur
Rolling $\|r\|$ slope (10-yr, HAC)	$+0.045\,\mathrm{yr^{-1}}$, $p < 0.001$	Gafsa

5. Discussion

5.1. Why satellite-based forecasting fails: information asymmetry

The failure of a standard satellite-and-machine-learning approach to outperform a naive trend baseline is consistent with a systemic property of the oasis rather than simply an algorithmic deficiency. A model that forecasts well by climate forecasts well because the climate signal is propagating into production; a system where the climate signal is absorbed by irrigation, by construction, does not produce a forecastable anomaly. The forecasting failure is therefore a quantitative measurement of the irrigation buffer, read as a statistical residual. This generalises the negative results reported for irrigated wheat by Tiedeman et al. (2022) and for cloudy landscapes by Farhat et al. (2023) to irrigated desert perennials at multi-governorate, multi-decade scale, under the leave-one-year-out cross-validation that Meyer et al. (2019) and Brinkhoff and Robson (2021) argue is mandatory for agricultural machine learning.

The persistence baseline failure adds an agronomic dimension. Alternate

bearing makes lag-1 anomalies actively misleading: an on-year predicts an off-year of opposite sign, so the naive baseline of zero anomaly outperforms the standard persistence competitor. In combination with the learned-model failure, this indicates that the state variables that would actually predict next year's deviation — pumping volumes, water-table depth, carbohydrate reserve carried over from the previous bearing cycle — are not in the covariates available to a satellite-based forecaster. What the satellite sees is the atmospheric forcing; what irrigated production reflects is the subsurface response. The two records are orthogonal by engineering design.

Tonnes-scale R^2 exceeding 0.99 is scale-driven: any model that predicts the per-governorate mean recovers most of the tonnes variance because the four governorates differ by roughly an order of magnitude. Tonnes-scale performance, in this setting, is not a meaningful measure of forecasting skill. The practical implication is that satellite products in oasis agriculture should not be evaluated on tonnes-scale predictive R^2, a metric that trend-fitting recovers by construction. They should be evaluated on how well they track the condition of the buffer that makes the tonnes-scale signal smooth. The remaining of the Discussion argues that a joint groundwater-and-coupling framework provides exactly this tracking capacity. A within-season earth-observation product targeted at per-orchard canopy state from Sentinel-2 remains plausible as a complementary tool for intra-season management; it answers a different question on different data and is not invalidated by the interannual forecasting result reported here (Claverie et al., 2018).

5.2. Decoupling as dynamic buffer monitoring

The main scientific contribution is the finding that climate–yield decoupling is not a binary property of an irrigation regime but a continuous dynamic that tracks the underlying water resource. The existing literature has established *that* intensive irrigation decouples yields from climate variability (Guillossou, 2025; Rigden et al., 2020; Jiang et al., 2020); it has not asked *when* that decoupling begins to weaken. Our temporal decoupling index answers exactly this question

on two-decade annual data that is now routinely available for most sub-national agricultural units globally. The computational machinery — rolling absolute correlation followed by a linear trend in the window centre — is standard; the contribution is the interpretive framework that connects the trend direction to irrigation-buffer degradation, and the operational application of that framework to fossil-aquifer-dependent agriculture. The index is dimensionless, requires only two time series, and is sign-aware: a positive slope indicates re-coupling as the buffer thins, a negative slope deepening decoupling as irrigation extends its reach.

The magnitude of the observed TWS decline is comparable to the satellite groundwater-depletion signatures documented by Rodell et al. (2009) for northern India and by Famiglietti (2014) for the broader semi-arid belt, confirming that the SASS region sits within the global pattern of irrigated-agriculture-driven aquifer stress. The most likely physical pathway linking aquifer decline to VPD sensitivity is declining well yield. As the water table drops — from near-surface artesian conditions in the early oasis era to depths exceeding 200 m in modern Continental Intercalaire boreholes (Mamou et al., 2006; Kinzelbach et al., 2021) — the hydraulic head available to drive irrigation flow decreases. Private wells with fixed-depth pumps lose capacity first; during peak-demand periods (July–August, when fruit-development VPD is at its annual maximum), marginal wells can no longer deliver the irrigation volume needed to match atmospheric demand. This produces a delivery constraint that is invisible in average years but binding in extreme-VPD years — exactly the pattern the re-coupling signal captures. Secondary pathways include rising pumping costs (deeper wells require more energy, which in some cases drives economically motivated under-irrigation) and water-quality degradation (salinisation of over-pumped wells can cause partial stomatal closure even when volumetric delivery is adequate (Ameur et al., 2017)). Distinguishing these mechanisms requires piezometric and orchard-level instrumentation that is beyond the scope of a satellite-and-statistics analysis.

The Kébili–Tozeur contrast sharpens the interpretation. Kébili exhibits

the institutional signature most likely to produce aquifer stress: Kébili's deep-aquifer exploitation (Table 3), the well proliferation documented in §2.1, and an area expansion financed entirely by private capital after the regulatory framework lapsed. The rising coupling trend (Table 3) is under HAC-corrected inference. Tozeur, by contrast, has been managed within formal institutional limits, its exploitation rate is comfortably below volumetric capacity, and its area expansion has been modest. Yet Tozeur's coupling slope shows a comparable trend on yield per hectare and actually slightly exceeds Kébili's (Table 3).

We frame the Tozeur finding as a hypothesis worth testing against longer time series and in-situ observations rather than as a confirmed result. One interpretation is that *operational* sustainability (the aquifer's capacity to meet peak irrigation demand during extreme atmospheric-water-demand years) can degrade before *volumetric* sustainability (total extraction exceeding total recharge). A system pumping at 70 % of renewable resources could still fail to deliver adequate irrigation during a one-in-ten-year VPD spike if the water table has fallen enough to constrain pump delivery rates. If this interpretation holds up against piezometric data and longer records, the safe operating margin for fossil-aquifer irrigation is substantially lower than the commonly cited 100 % extraction-to-recharge ratio. The two-period bootstrap confidence interval around Tozeur's $\Delta|r|$ crosses zero on the available sample; the rolling-window slope, which aggregates information across the full record, is where the statistical support for the Tozeur finding sits.

A final point on the apparent tension between the coupling result and the production trajectory. Kébili yields per hectare have more than doubled (from 3.7 to 8.2 $\mathrm{t\,ha^{-1}}$, period means) over the study period, yet we claim the buffer is thinning. The two signals live at different time scales. The level of yield tracks cumulative investment — new wells, new pumps, maturing palms — and is monotonically increasing. The interannual variability of yield, once the level trend is removed, tracks the year-to-year balance between atmospheric demand and the aquifer's capacity to meet it. A system can capitalise its productive mean while its interannual resilience erodes; indeed, the capitalisation is what

has driven the water table down (Mamou et al., 2006; Ameur et al., 2017; Kinzelbach et al., 2021).

5.3. Policy implications

The results translate into three concrete monitoring implications for Tunisian water and agriculture agencies. First, the VPD–yield-per-hectare decoupling index can be computed annually from publicly available data for each governorate and integrated into CRDA's existing aquifer-bulletin reporting as a single-number coupling indicator. We propose an illustrative threshold of $|r| > 0.5$ sustained across three consecutive windows as a possible monitoring trigger; this value requires validation against independent aquifer indicators (piezometric depth, pump-energy records, salinity) before operational adoption. Under that illustrative threshold, Kébili has already crossed in recent windows. Second, GRACE-based annual terrestrial water storage should be tracked alongside CRDA's extraction accounting. The satellite signal is governance-independent, catches unreported extraction that CRDA bulletins under-count (World Bank Group and Ministry of Agriculture, Tunisia, 2024), and provides an integral check on permit compliance at the scale at which permits are actually issued. Third, Kébili specifically requires a functioning well registry and metered extraction at the scale of commercial pumps. The CRDA anchor counts differ by a factor whose midpoint is unknown because an unquantified fraction of private wells is informal; completion of the registry is a precondition for any enforcement regime. The urgency of this recommendation is underscored by the governance contrast within the study region itself: Gabès established a safeguard zone in 2017 that prohibits new deep wells beyond 50 m (Hassenforder et al., 2025), yet Kébili — where overexploitation is three times more severe — has no equivalent regulatory protection. The participatory governance processes recently initiated in Kébili (Ferchichi et al., 2024) offer a promising pathway, but they require the monitoring infrastructure that a functioning well registry and the decoupling index could provide.

The well proliferation driving this buffer degradation has been amplified by

broader economic forces: nationally, over 66 % of deep agricultural boreholes currently operate without formal authorisation (ONAGRI, 2023), and declining pumping costs — driven partly by the transition to solar-powered irrigation — have removed the traditional economic brake on extraction volumes. Recent legislative responses, including the regularisation pathway established in the 2025 Finance Law (Article 81; République Tunisienne, 2024), create a potential registry but risk legitimising unsustainable extraction unless paired with mandatory monitoring and recharge-linked quotas. The national-scale headline exploitation rate of 126–129 % reported by the Tunisian Court of Audit is an arithmetic mean over a landscape in which Kébili alone is at 229 % — another illustration of why national averages mask local crises.

These recommendations align with the policy frameworks of Chebil et al. (2018) and Kinzelbach et al. (2021) for overexploited fossil aquifers, and with the constitutional-rights and socio-hydrological analyses of Omar (2025) and Ameur et al. (2017). Our contribution is evidentiary — the quantitative detection of a coupling shift consistent with an aquifer threshold approach — rather than prescriptive; the choice of regulatory instrument is a policy decision that sits beyond the scope of an earth-observation analysis. We note that these recommendations presuppose institutional capacity that CRDA offices in southern Tunisia currently lack; the monitoring framework we propose is designed to be computationally lightweight (two time series, publicly available data, annual update) precisely to lower this barrier.

5.4. Limitations

Twenty-three years of annual data is a small sample for the statistical tests employed. The per-governorate rolling-slope inference retains power through HAC correction on overlapping windows; the two-period bootstrap confidence intervals, in contrast, are wide and cross zero on sub-samples of eleven-versus-twelve observations. We have therefore relied on the rolling-window trend as the primary inferential test and treated the two-period statistic as a descriptive complement.

GRACE mascon resolution of approximately 3° exceeds the four-governorate footprint, so the TWS signal integrates across all governorates and partially beyond, and cannot distinguish intra-governorate aquifer structure (for example, Nefzaoua versus Chott-margin Kébili). The CRDA extraction-weighted disaggregation partially compensates but does not fully resolve this; governorate-resolved depletion rates should therefore be read as the regional signal disaggregated by extraction share, not as independent mascon-resolved measurements. The CRDA extraction weights themselves are derived from the 2020–2024 bulletins (the earliest with complete coverage) and are projected backwards under a proportional-stability assumption that we cannot directly verify before 2020; time-varying weights and GRACE downscaling products (Hamou-Ali et al., 2025; Chen et al., 2021; Suryawanshi et al., 2025) offer natural extensions.

The palm-fraction correction for Gabès and Gafsa is a 2024 snapshot. We have restricted the yield-per-hectare analysis to Tozeur and Kébili, where the fraction is effectively 1.0 by construction, for precisely this reason.

The claim that VPD has become informative about Kébili yield anomalies is not a claim that VPD causes those anomalies. The rising coupling is consistent with a thinning subsurface buffer, but could in principle reflect phenology shifts, changes in varietal mix, or canopy-level stomatal adaptation. Disambiguation requires eddy-covariance or sap-flow instrumentation on a sub-sample of Kébili orchards. The ONAGRI production series is reported as a total across date varieties rather than separately for Deglet-Nour and common varieties; shifts in varietal composition could in principle contribute to the late-period yield-per-hectare signal, though the Deglet-Nour share is known to be dominant in Tozeur and Kébili (Al-Omran et al., 2019; Belloumi and Matoussi, 2006).

The ONAGRI production series carries known limitations of governorate-level agricultural statistics in the MENA region: inspection of the 23-year four-governorate record reveals four cases of identical consecutive annual values (Gabès 2021–2022 and 2023–2024; Gafsa 2003–2004 and 2021–2022), suggesting carried-forward estimates in years where fresh measurement was unavailable, and a heavy rounding pattern in the Kébili series (83 % of values are exact

multiples of 1,000 t). These quality concerns do not invalidate the decoupling analysis, which operates on detrended anomalies and is therefore insensitive to trend-level reporting biases, but they may degrade the precision of individual-year anomaly estimates and contribute to the wide bootstrap intervals on the two-period contrast.

Across the full exploratory grid (4 governorates × 4 climate features × 2 targets = 32 cells) no individual cell reaches Benjamini–Hochberg-adjusted significance at $q < 0.05$. The Kébili VPD–yield/ha result is supported not by an FDR-adjusted p-value on the two-period contrast but by the convergence of the HAC-corrected rolling-window trend ($p < 0.001$ at Kébili, Tozeur, and Gafsa), the seven-feature placebo panel, and the physical triangulation with GRACE depletion and well-proliferation evidence.

The trailing-only detrending method collapses the signal to near zero, driven by initialisation noise in the first 2–4 years of the series; this sensitivity is documented in Supplementary Table S2. Quadratic detrending preserves the Kébili and Tozeur findings ($\Delta|r| = +0.41$ and $+0.43$) but reduces Gafsa's two-period contrast to near zero, although Gafsa's rolling-window slope remains significant.

The yield anomaly is defined using a linear trend fitted to the full 2002–2024 record, including the 2021–2024 test period. This is appropriate for the retrospective decoupling analysis but means the satellite-based forecasting comparison in §4.1 is not a strictly operational out-of-sample evaluation; it should be read as a diagnostic demonstration of the irrigation buffer's effectiveness rather than a forecast skill benchmark.

6. Conclusions

Across the four date-palm governorates of southern Tunisia, satellite/climate-based yield-anomaly forecasting fails to outperform a naive trend baseline. The failure is consistent with a functioning irrigation buffer that suppresses the climate-to-yield signal by design. What the satellite sees is the atmosphere; what irrigated production reflects is the subsurface capacity to compensate for

atmospheric demand.

GRACE and GRACE-FO terrestrial water storage document sustained groundwater depletion over the 22-year study period, with the aquifer approximately stable through the mid-2000s and then declining at a rate consistent with the pumping regime recorded by CRDA accounting and national audits.

A rolling-window temporal decoupling index identifies Kébili and Tozeur as governorates where climate–yield coupling is rising robustly; Gafsa shows the same signature under linear detrending but not under quadratic detrending, and is reported tentatively. The Kébili signal survives area normalisation and is robust to break-year choice and placebo-feature alternatives. The convergence of rising VPD sensitivity with groundwater depletion and well proliferation gives the coupling signal an operational meaning: the irrigation buffer is thinning in exactly the governorates where extraction pressure is greatest.

Together, these findings reframe the role of satellite earth observation in aquifer-dependent irrigated systems. The satellite/climate record cannot forecast yields in an engineered oasis, but it can monitor the cost of the engineering and detect when the underlying resource can no longer sustain it. The temporal decoupling index, combined with GRACE terrestrial water storage, provides a monitoring capacity that is directly applicable to CRDA's existing aquifer-bulletin framework and can be computed annually from publicly available data. Analogous aquifer-dependent systems — from the Al-Hasa oasis complex to qanat-fed systems in Iran to the Murray–Darling Basin — face comparable trajectories, and the framework proposed here offers an early-warning tool that operates on data already available in most of these systems.

Data availability

The compiled datasets and analysis code are available at `https://github.com/tanitdata/DatePalm` and archived at `https://doi.org/10.5281/zenodo.20172850`. Satellite data were extracted through Google Earth Engine; GRACE and GRACE-FO mascons are from NASA's

Physical Oceanography Distributed Active Archive Center (PO.DAAC). Ground-truth datasets from the Tunisian agricultural open data portal (`https://catalog.agridata.tn`) were accessed via the TanitData MCP server (Gasmi, 2026). All data were accessed between January and March 2026.

References

Aguilar, A.L., Flores, H., Crespo, G., Marín, M.I., Campos, I., Calera, A., 2018. Performance assessment of MOD16 in evapotranspiration evaluation in northwestern Mexico. Water 10, 901. doi:10.3390/w10070901.

Al-Omran, A., Eid, S., Alshammari, F., 2019. Crop water requirements of date palm based on actual applied water and Penman–Monteith calculations in Saudi Arabia. Applied Water Science 9, 69. doi:10.1007/s13201-019-0936-6.

Alikhani-Koupaei, M., Soleimani Aghdam, M., Faghih, S., 2020. Physiological aspects of date palm loading and alternate bearing under regulated deficit irrigation compared to cutting back of bunch. Agricultural Water Management 232, 106035. doi:10.1016/j.agwat.2020.106035.

Ameur, F., Amichi, H., Kuper, M., Hammani, A., 2017. Specifying the differentiated contribution of farmers to groundwater depletion in two irrigated areas in North Africa. Hydrogeology Journal 25, 1579–1591. doi:10.1007/s10040-017-1569-1.

Belloumi, M., Matoussi, M.S., 2006. A stochastic frontier approach for measuring technical efficiencies of date farms in southern Tunisia. Agricultural and Resource Economics Review 35, 285–298. doi:10.1017/S1068280500006730.

Besser, H., Mokadem, N., Redhouania, B., Rhimi, N., Khlifi, F., Ayadi, Y., Omar, Z., Bouajila, A., Hamed, Y., 2017. GIS-based evaluation of groundwater quality and estimation of soil salinization and land degradation risks

in an arid Mediterranean site (SW Tunisia). Arabian Journal of Geosciences 10, 350. doi:10.1007/s12517-017-3148-0.

Brinkhoff, J., Robson, A.J., 2021. Block-level macadamia yield forecasting using spatio-temporal datasets. Agricultural and Forest Meteorology 303, 108369. doi:10.1016/j.agrformet.2021.108369.

Chebil, A., Kahil, T., Oueslati, B., 2018. Policy measures for reducing aquifer depletion in a context of climate change: The case of the coastal area of Cap-Bon. Technical Report nm1804c. IIASA Working Papers. URL: https://pure.iiasa.ac.at/id/eprint/15779/.

Chen, Z., Zheng, W., Yin, W., Li, X., Zhang, G., Zhang, J., 2021. Improving the spatial resolution of GRACE-derived terrestrial water storage changes in small areas using the machine learning spatial downscaling method. Remote Sensing 13, 4760. doi:10.3390/rs13234760.

Claverie, M., Ju, J., Masek, J.G., Dungan, J.L., Vermote, E.F., Roger, J.C., Skakun, S.V., Justice, C., 2018. The harmonized Landsat and Sentinel-2 surface reflectance data set. Remote Sensing of Environment 219, 145–161. doi:10.1016/j.rse.2018.09.002.

Faci, M., Benziouche, S.E., 2021. Contribution to monitoring the influence of air temperature on some phenological stages of the date palm (cultivar 'deglet Nour') in Biskra. Journal of the Saudi Society of Agricultural Sciences 20, 248–256. doi:10.1016/j.jssas.2021.02.004.

Famiglietti, J.S., 2014. The global groundwater crisis. Nature Climate Change 4, 945–948. doi:10.1038/nclimate2425.

Farhat, L., Manakos, I., Sylaios, G., Kalaitzidis, C., 2023. A modified version of the direct sampling method for filling gaps in landsat 7 and sentinel 2 satellite imagery in the coastal area of rhone river. Remote Sensing 15, 5122. doi:10.3390/rs15215122.

Ferchichi, I., Mekki, I., Taouajouti, N., Faysse, N., Zairi, A., Chaibi, T., ElGuedri, I., Ben Ali, H., Sghairoun, M., Imache, A., Barbe, A., 2024. La visualisation spatiale: un outil de dialogue sur la gestion des eaux souterraines dans les palmeraies de Kébili, Tunisie. Cahiers Agricultures 33, 24. doi:10.1051/cagri/2024019.

Gao, F., Feng, G., Ouyang, Y., Wang, H., Fisher, D., Adeli, A., Jenkins, J., 2017. Evaluation of reference evapotranspiration methods in arid, semiarid, and humid regions. Journal of the American Water Resources Association 53, 791–808. doi:10.1111/1752-1688.12530.

Gasmi, T., 2026. tanitdata: Domain-adapted MCP server for Tunisia's agricultural open data. Software, https://github.com/tanitdata/agridata-mcp. MCP server providing AI-mediated access to catalog.agridata.tn with semantic layer for vocabulary bridging.

Grossiord, C., Buckley, T.N., Cernusak, L.A., Novick, K.A., Poulter, B., Siegwolf, R.T.W., Sperry, J.S., McDowell, N.G., 2020. Plant responses to rising vapor pressure deficit. New Phytologist 226, 1550–1566. doi:10.1111/nph.16485.

Guillossou, M., 2025. The Impact of Climate Change on Yield Growth and the Mitigating Role of Irrigation in the Corn Belt. EconomiX Working Paper 2025-4. University of Paris Nanterre, EconomiX. URL: https://ideas.repec.org/p/drm/wpaper/2025-4.html.

Haj-Amor, Z., Acharjee, T.K., Dhaouadi, L., Bouri, S., 2020. Impacts of climate change on irrigation water requirement of date palms under future salinity trend in coastal aquifer of Tunisian oasis. Agricultural Water Management 228, 105843. doi:10.1016/j.agwat.2019.105843.

Hamou-Ali, Y., Karmouda, N., Mohsine, I., Bouramtane, T., Kacimi, I., Tweed, S., Tahiri, M., Kassou, N., El Bilali, A., Chafki, O., Ezzaouini, M.A., Laraichi, S., Zerouali, A., Leblanc, M., 2025. Downscaling GRACE total water storage

data using random forest: a three-round validation approach under drought conditions. Frontiers in Water 7, 1545821. doi:10.3389/frwa.2025.1545821.

Hao, X., Sun, F., Zhang, J., Ci, M., Li, Y., Fan, X., Liang, Q., Li, X., 2025. Vapor pressure deficit governs oasis cooling efficiency and drought intensified water-heat tradeoffs in arid regions. Journal of Hydrology 661, 133804. doi:10.1016/j.jhydrol.2025.133804.

Hassenforder, E., et al., 2025. Identifying solutions to face groundwater over-exploitation and degradation: A policy design experiment in Tunisia. Water and Environment Journal doi:10.1111/wej.12986.

Heydari, M.M., Heydari, M., 2014. Calibration of Hargreaves–Samani equation for estimating reference evapotranspiration in semiarid and arid regions. Archives of Agronomy and Soil Science 60, 695–713. doi:10.1080/03650340.2013.821588.

Jiang, Y., Wang, X., Ti, J., Lu, Z., Yin, X., Chu, Q., Lei, Y., Chen, F., 2020. Assessment of winter wheat water-saving potential in the groundwater over-exploitation district of the North China Plain. Agronomy Journal 112, 44–55. doi:10.1002/agj2.20041.

Kharroubi, A., Farhat, S., Agoubi, B., Lakhbir, Z., 2014. Assessment of water qualities and evidence of seawater intrusion in a deep confined aquifer: case of the coastal Djeffara aquifer (southern Tunisia). Journal of Water Supply: Research and Technology — Aqua 63, 76–84. doi:10.2166/aqua.2013.105.

Kinzelbach, W., Wang, H., Li, Y., Wang, L., Li, N., 2021. Groundwater Over-exploitation and Contamination: The Need for a Paradigm Shift. Springer Water. doi:10.1007/978-981-16-5843-3.

Kross, A., Znoj, E., Callegari, D., Kaur, G., Sunohara, M., Lapen, D.R., McNairn, H., 2020. Using artificial neural networks and remotely sensed data to evaluate the relative importance of variables for prediction of within-field corn and soybean yields. Remote Sensing 12, 2230. doi:10.3390/rs12142230.

Landerer, F.W., Flechtner, F.M., Save, H., Webb, F.H., Bandikova, T., Bertiger, W.I., Bettadpur, S.V., Byun, S.H., Dahle, C., Dobslaw, H., Fahnestock, E., Harvey, N., Kang, Z., Kruizinga, G.L.H., Loomis, B.D., McCullough, C., Murböck, M., Nagel, P., Paik, M., Pie, N., Poole, S., Strekalov, D., Tamisiea, M.E., Wang, F., Watkins, M.M., Wen, H.Y., Wiese, D.N., Yuan, D.N., 2020. Extending the global mass change data record: GRACE Follow-On instrument and science data performance. Geophysical Research Letters 47, e2020GL088306. doi:10.1029/2020GL088306.

Lobell, D.B., Roberts, M.J., Schlenker, W., Braun, N., Little, B.B., Rejesus, R.M., Hammer, G.L., 2014. Greater sensitivity to drought accompanies maize yield increase in the U.S. Midwest. Science 344, 516–519. doi:10.1126/science.1251423.

Lundberg, S.M., Lee, S.I., 2017. A unified approach to interpreting model predictions, in: Advances in Neural Information Processing Systems, pp. 4765–4774.

Malone, B.P., Minasny, B., McBratney, A.B., 2022. Identifying causes of crop yield variability with interpretive machine learning. Computers and Electronics in Agriculture 192, 106632. doi:10.1016/j.compag.2021.106632.

Mamou, A., Besbes, M., Abdous, B., Latrech, D.J., Fezzani, C., 2006. North western Sahara aquifer system (NWSAS), in: Foster, S., Loucks, D.P. (Eds.), Non-Renewable Groundwater Resources: A Guidebook on Socially-Sustainable Management for Water-Policy Makers. UNESCO, pp. 68–74.

Mekki, I., Ferchichi, I., Taoujouti, N., Faysse, N., Zairi, A., 2022. Oasis extension trajectories in Kebili territory, Southern Tunisia: drivers of development and actors' discourse. New Medit 21, nm2205f. doi:10.30682/nm2205f.

Meyer, H., Reudenbach, C., Wöllauer, S., Nauss, T., 2019. Importance of spatial predictor variable selection in machine learning applications — moving from data reproduction to spatial prediction. Ecological Modelling 411, 108815. doi:10.1016/j.ecolmodel.2019.108815.

Mu, Q., Zhao, M., Running, S.W., 2011. Improvements to a MODIS global terrestrial evapotranspiration algorithm. Remote Sensing of Environment 115, 1781–1800. doi:10.1016/j.rse.2011.02.019.

National Court of Audit of Tunisia, 2019. Report on Groundwater Exploitation in High-Risk Zones. Technical Report. Tunisian State Archives.

Observatoire du Sahara et du Sahel (OSS), 2002. Système aquifère du Sahara septentrional: Gestion commune d'un bassin transfrontalier. Technical Report. OSS. Tunis, Tunisie.

Omar, A., 2025. Securing Constitutional Rights to Water: Policy Solutions. Technical Report. Carnegie Endowment for International Peace.

ONAGRI, 2023. Annuaire des statistiques agricoles. Technical Report. Observatoire National de l'Agriculture. Tunis.

Rashid, M., Bari, B.S., Yusup, Y., Kamaruddin, M.A., Khan, N., 2021. A comprehensive review of crop yield prediction using machine learning approaches with special emphasis on palm oil yield prediction. IEEE Access 9, 63406–63439. doi:10.1109/ACCESS.2021.3075159.

Rigden, A.J., Mueller, N.D., Holbrook, N.M., Pillai, N., Huybers, P., 2020. Combined influence of soil moisture and atmospheric evaporative demand is important for accurately predicting US maize yields. Nature Food 1, 127–133. doi:10.1038/s43016-020-0028-7.

Rodell, M., Velicogna, I., Famiglietti, J.S., 2009. Satellite-based estimates of groundwater depletion in India. Nature 460, 999–1002. doi:10.1038/nature08238.

République Tunisienne, 2024. Loi n° 2024-48 du 9 décembre 2024, portant loi de finances pour l'année 2025. Journal Officiel de la République Tunisienne, n° 149. Article 81: régularisation des forages agricoles profonds non autorisés.

Sabo, F., Meroni, M., Piles, M., Claverie, M., Ferreira, F., Van Den Berg, E., Collivignarelli, F., Rembold, F., 2025. From rows to yields: How foundation models for tabular data simplify crop yield prediction. arXiv:2506.19046. URL: https://arxiv.org/abs/2506.19046, arXiv:2506.19046.

Suryawanshi, M.R., Kumar, K.S., Shakya, A., Chander, S., Nikam, B., Dasika, N.K., Vishwakarma, B.D., 2025. On the efficacy of downscaled GRACE total water storage products. EGUsphere preprint, doi:10.5194/egusphere-2025-2888.

Tiba, H., Dhaouadi, L., Karbout, N., Al-Omran, A., Sellami, M.H., 2025. Irrigation management and water requirements of date palm in three oases of tunisia. Journal of Oasis Agriculture and Sustainable Development 7, 1–12. doi:10.56027/JOASD.152025.

Tiedeman, K., Chamberlin, J., Kosmowski, F., Ayalew, H., Sida, T., Hijmans, R.J., 2022. Field data collection methods strongly affect satellite-based crop yield estimation. Remote Sensing 14, 1995. doi:10.3390/rs14091995.

Wang, K., Feng, J., Zhao, Z., Han, B., 2023. Analysis of winter anomaly and annual anomaly based on regression approach. Remote Sensing 15, 4968. doi:10.3390/rs15204968.

World Bank Group, Ministry of Agriculture, Tunisia, 2024. Thirsty Tunisia: Our Water Between Plunder, Depletion, and Patchwork Policies. Technical Report. National Investigations Report.

S1. Data source identifiers and access

The satellite and reanalysis products used in the study are listed below with full version identifiers. All products were accessed between January and March 2026 through Google Earth Engine or NASA's Physical Oceanography Distributed Active Archive Center (PO.DAAC).

- **MODIS MOD13A2 NDVI**, Collection 6.1, 1 km, 16-day composite; scaling factor 0.0001.
- **MODIS MOD11A2 LST**, Collection 6.1, 1 km, 8-day composite; Kelvin $\times 0.02 - 273.15$ to convert to degrees Celsius.
- **MODIS MOD16A2 ET**, Collection 6.1, 500 m (excluded: 18 % valid-pixel coverage).
- **ERA5-Land monthly aggregates**, 9 km: 2 m temperature, 2 m dewpoint, total precipitation, surface net solar radiation, 10 m wind u and v components.
- **CHIRPS v2.0**, 5 km, daily precipitation aggregated to monthly totals, maximum daily precipitation, and rain-day counts.
- **GRACE/GRACE-FO JPL Mascon** RL06.3M v04 CRI (Coastline Resolution Improvement filter), approximately 3° mascons, monthly.
- **Sentinel-2 L2A**, 10 m, 2015–2024 (excluded from annual analysis; retained for intra-season work).
- **SRTM v003**, 30 m, static elevation.
- **SoilGrids 2.0**, 250 m, clay, sand, and soil organic carbon at 0–5 cm.

Ground-based datasets were obtained through the Tunisian agricultural open data portal (`https://catalog.agridata.tn`), accessed via the TanitData MCP server (Gasmi, 2026):

- **ONAGRI production records** (ONAGRI 2023 annuaire), governorate-level annual date-palm tonnage, 2002–2024.
- **CRDA aquifer bulletins**, 2020–2024, providing resources, extraction volumes, exploitation rates, and well counts by governorate and aquifer type.
- Three Kébili private-well anchor counts were verified against the Court of Audit (National Court of Audit of Tunisia, 2019) and the World Bank "Thirsty Tunisia" investigation (World Bank Group and Ministry of Agriculture, Tunisia, 2024): approximately 3,700 (2008), 7,900 (2017), and 10,600 (2023).

S2. Hargreaves reference evapotranspiration

Reference evapotranspiration (ET_0) is computed with the temperature-and-radiation-based Hargreaves formulation, which is well-calibrated for arid Mediterranean conditions (Heydari and Heydari, 2014; Gao et al., 2017) and does not require vapour-pressure or wind inputs:

$$\mathrm{ET}_0 = 0.0023\, R_a\, (T_{\max} - T_{\min})^{0.5}\, (T_{\mathrm{mean}} + 17.8), \tag{B.1}$$

with ET_0 in $\mathrm{mm\,day^{-1}}$, extraterrestrial solar radiation R_a in $\mathrm{mm\,day^{-1}}$ equivalent, and air temperatures in degrees Celsius. The Hargreaves approach is preferred here over the Penman–Monteith reference because the missing MODIS MOD16A2 product would have provided the radiation and aerodynamic terms; the temperature-only Hargreaves substitute is robust and independently calibrated for this region.

S3. Model hyperparameters

Table S1 reports the hyperparameter specifications for the three model families used in the forecasting test. All models were trained under leave-one-year-out cross-validation on the 2002–2020 training window (19 governorate-years

per fold × 4 governorates = 76 training samples per fold) with a held-out 2021–2024 test set. The 111-feature full configuration includes the annual aggregates of all engineered variables (see Section S4); the 12-feature sparse configuration retains the variables most closely tied to date-palm agronomy.

Table S1: Model hyperparameters.

Model	Specification
Ridge (linear regression with L_2 regularisation)	Regularisation strength α selected by inner cross-validation over a log-spaced grid from 10^{-3} to 10^{3}.
Random Forest	500 trees; maximum depth 6; minimum 5 samples per leaf; $\sqrt{p}$ features considered per split.
XGBoost	300 trees; maximum depth 4; learning rate $\eta = 0.05$; subsample fraction 0.8 (rows) and 0.6 (columns per tree); L_1 regularisation $\alpha = 2.0$; L_2 regularisation $\lambda = 10.0$; minimum child weight 5.
SHAP	Tree SHAP attribution (Lundberg and Lee, 2017; Malone et al., 2022) applied to XGBoost fits to inspect feature-importance stability across leave-one-year-out folds.

S4. Feature engineering and predictor sets

Predictors were derived from the raw monthly satellite and reanalysis products to capture agronomically interpretable signals on annual and phenological-window timescales.

- Growing degree days at base 18°C (GDD_{18}): monthly $\mathrm{GDD}_{18} = \max(0, T_{\mathrm{mean}} - 18\,^{\circ}\mathrm{C}) \times \mathrm{days\_in\_month}$, with T_{mean} approximated by the mean of MODIS LST day and night. Base temperature 18°C follows the date-palm phenology calibration of Faci and Benziouche (2021).
- Vapour pressure deficit (VPD): saturation vapour pressure from the Tetens formulation, $e_{\mathrm{sat}} = 0.6108 \exp\big(17.27T/(T + 237.3)\big)$,

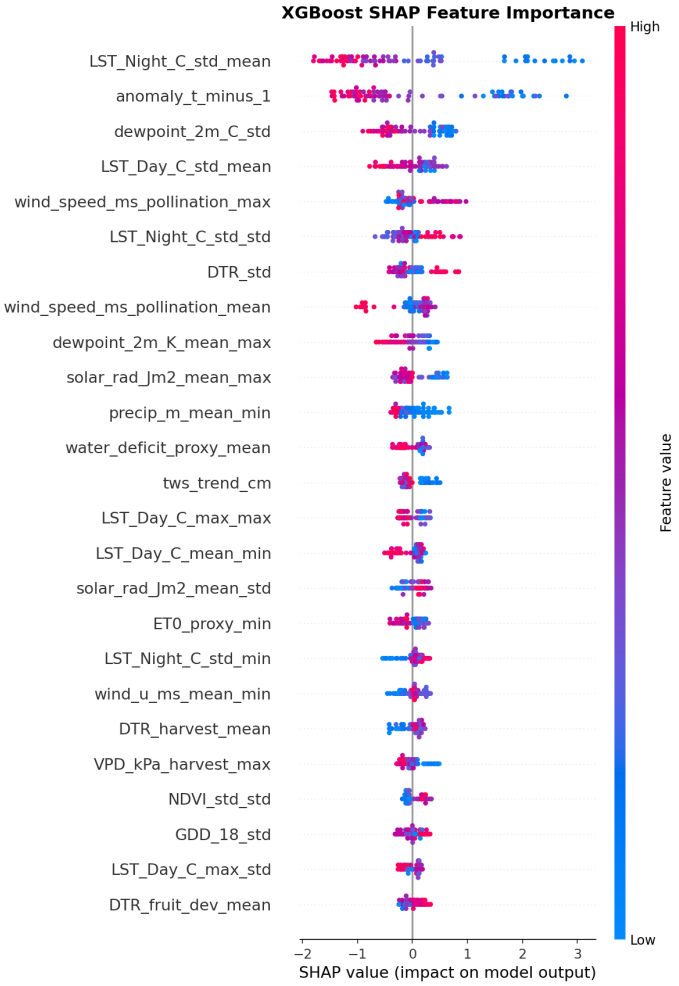

Figure S1: SHAP feature-attribution summary for XGBoost. Top features swap across leave-one-year-out folds and attribution magnitudes are within run-to-run noise, consistent with the absence of a learnable anomaly signal.

evaluated at ERA5-Land 2 m temperature and 2 m dewpoint; VPD $= \max(0, e_{\mathrm{sat}}(T) - e_{\mathrm{sat}}(T_{\mathrm{dew}}))$. Aggregated over the annual cycle and over three phenological windows: pollination (March–April), fruit development (May–August), and harvest (September–November).

- Diurnal temperature range: MODIS LST day minus LST night.
- Wind speed ($\sqrt{u^2 + v^2}$) and sirocco-month counts (months where maximum wind speed exceeds $8\,\mathrm{m\,s^{-1}}$ and MODIS LST day maximum exceeds 40 °C during March–August).
- Heat-stress months: count of months where MODIS LST day maximum exceeds 45 °C.
- Hargreaves ET_0 proxy (Section S2).
- Water-deficit proxy: monthly precipitation minus ET_0, annual sum.
- Phenological-window aggregates of NDVI, GDD, VPD, DTR, and wind.

Correlation filtering removed predictors with pairwise $|r| > 0.95$, yielding a 111-feature full set from the roughly 150 engineered variables. The 12-feature sparse configuration retains: lag-1 anomaly, TWS linear-trend slope, mean NDVI during fruit development, annual GDD_{18}, mean VPD during fruit development, heat-stress months, diurnal temperature range during pollination, annual rain days, sirocco months, annual total precipitation, annual-mean shortwave radiation, and annual Hargreaves ET_0. Static soil and terrain variables were excluded because they act as time-invariant governorate identifiers rather than temporal predictors.

S5. Robustness analyses

All robustness analyses target the two-period $\Delta|r|$ for Kébili between fruit-development-window VPD and yield-per-hectare anomaly.

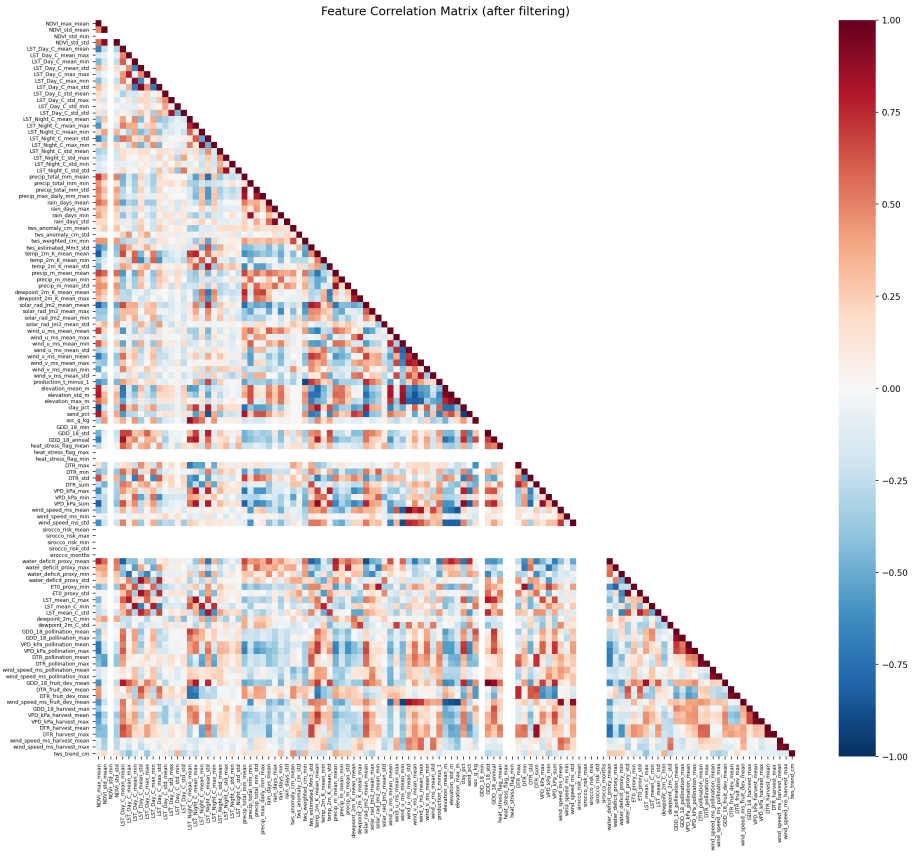

Figure S2: Pairwise Pearson correlation heatmap of the 111-feature predictor set used by the forecasting models. The $|r| > 0.95$ filter removes the most strongly co-varying pairs.

Table S2: Detrending-method sensitivity for $\Delta|r|$ (VPD fruit-development versus yield-per-hectare anomaly, break year 2012).

Detrending method (yield series)	Kébili $\Delta\|r\|$	Tozeur $\Delta\|r\|$	Gafsa $\Delta\|r\|$	Notes
Linear (primary)	+0.444	+0.604	+0.471	OLS fit on full 2002–2024 series
Quadratic (new)	**+0.413**	**+0.425**	**−0.025**	OLS fit including year^2; tests for nonlinear co-trend
5-year centred rolling	+0.462	—	—	Uses future information near endpoints
5-year trailing rolling	−0.054	—	—	Early-period initialisation noise
First-differencing	+0.140	—	—	No trend model; absorbs low-frequency signal

The Kébili and Tozeur findings are robust to quadratic detrending of the yield series: $\Delta|r|$ remains positive at +0.413 and +0.425 respectively, and the Kébili rolling-window slope under quadratic-detrended yield is $+0.028\,\mathrm{yr}^{-1}$ with HAC-corrected $p < 0.001$. Gafsa's two-period $\Delta|r|$ collapses to −0.025 under quadratic detrending — consistent with a substantial portion of Gafsa's two-period contrast being attributable to a co-curving yield trajectory — although Gafsa's rolling-window slope remains significant ($p = 0.003$). The Kébili–Tozeur findings are therefore not artefacts of residual nonlinear co-trends between VPD and yield; the Gafsa finding requires more cautious interpretation. The trailing-window detrending result is reported only for Kébili, where the early-period initialisation collapse is most severe.

Table S3: Break-year sensitivity for Kébili $\Delta|r|$ under linear detrending.

Break year	n early	n late	r early	r late	$\Delta\|r\|$
2010	9	14	+0.165	+0.440	+0.275
2011	10	13	+0.188	+0.431	+0.243
2012 (default)	11	12	−0.038	+0.482	+0.444
2013	12	11	+0.144	+0.333	+0.189
2014	13	10	+0.150	+0.330	+0.180
2015	14	9	+0.161	+0.260	+0.098

$\Delta|r|$ is positive at every tested break year. The 2012 split is retained as the default two-period contrast for the VPD analysis because it divides the 2002–2024 record into approximately equal early and late periods; break-year sensitivity from 2010 to 2015 is reported above. The GRACE structural-break test (main text, §4.2) places the depletion-rate break at 2007, an independent quantity.

VPD's $\Delta|r|$ exceeds all seven climatically neutral placebos.

The rolling-window slope is reported with Newey–West heteroskedasticity- and autocorrelation-consistent (HAC) standard errors using a Bartlett kernel at lag $w - 1 = 9$, the natural bandwidth when adjacent 10-year windows share

Table S4: Placebo-feature $\Delta|r|$ against Kébili yield-per-hectare anomaly (linear detrending, break 2012).

Feature	r early	r late	$\Delta\|r\|$
VPD fruit-development mean (focal)	-0.038	$+0.482$	$+0.444$
Std of max daily precipitation	-0.093	$+0.466$	$+0.374$
Annual mean wind speed	-0.053	$+0.256$	$+0.203$
Harvest-window DTR	-0.102	$+0.198$	$+0.096$
Annual NDVI std	-0.120	-0.105	-0.015
Annual min dewpoint	$+0.114$	$+0.094$	-0.020
Annual rain days	-0.641	-0.429	-0.212
Std of mean solar radiation	$+0.373$	-0.036	-0.337

nine underlying years. The resulting HAC-corrected p-values for the four per-governorate rolling slopes are Tozeur $p = 0.011$, Kébili $p = 3.7 \times 10^{-6}$, Gafsa $p = 1.0 \times 10^{-7}$, Gabès $p = 0.30$.

For the two-period $\Delta|r|$ we report a paired bootstrap 95 % confidence interval, drawing 5,000 resamples with replacement separately from the early ($n = 11$) and late ($n = 12$) periods. For Kébili the bootstrap-mean $\Delta|r|$ is $+0.279$ with a 95 % CI of $[-0.30, +0.75]$; 83 % of resamples produce $\Delta|r| > 0$. For Tozeur the bootstrap-mean is $+0.33$ with a 95 % CI of $[-0.31, +0.79]$; 87 % of resamples are positive. Both intervals cross zero because each period contains only about a dozen observations, which is why the rolling-window trend — which aggregates information across the full record — is the primary inferential test.

A block bootstrap on the underlying VPD and yield anomaly series (5,000 replicates, block length equal to the window length of 10 years) returns a rolling-slope distribution centred on zero with a 95 % CI of $[-0.043, +0.040]$. This is not a contradiction of the HAC-corrected significance: block-bootstrap resampling by construction randomises the temporal ordering of the blocks, and the decoupling claim is about the temporal evolution of the coupling. A resampling scheme that discards time necessarily discards the signal. The HAC inference,

which preserves the time ordering and corrects for within-series autocorrelation, is the appropriate test for a temporal-trend claim.

An exploratory scan covered 4 governorates $\times$ 4 candidate climate features $\times$ 2 targets $= 32$ cells. Under a Benjamini–Hochberg correction across all 32 cells no single cell reaches $q < 0.05$, reflecting the limited power of the two-period test on sub-samples of about a dozen years. The VPD–Kébili–yield/ha cell ranks eighth by uncorrected p-value. The paper's primary statistical support is the rolling-window trend rather than the two-period test.

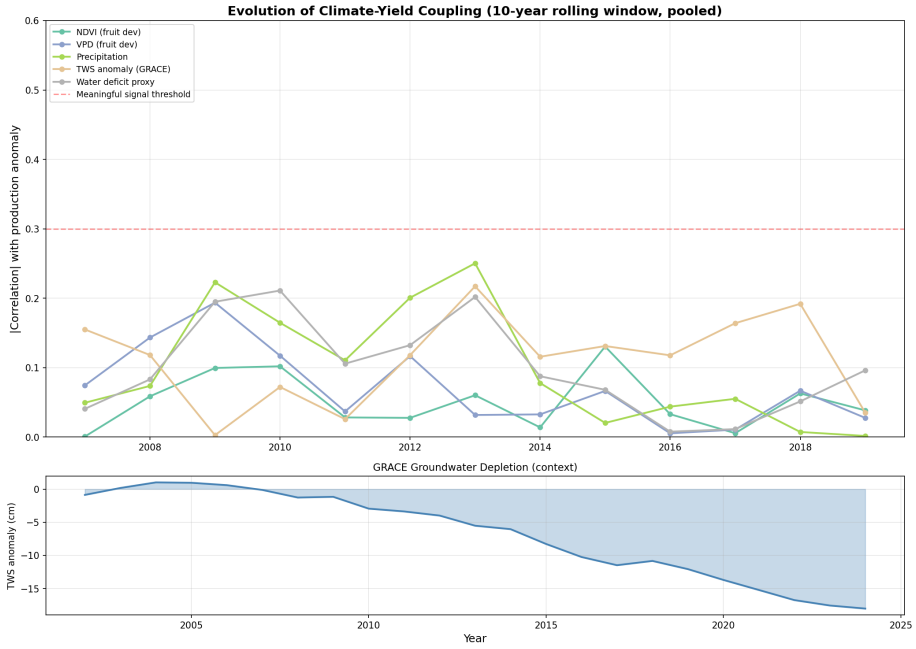

Figure S3: Pooled rolling 10-year correlation between fruit-development-window VPD and yield/ha anomaly across the four governorates combined.

S6. CRDA cross-check of the persistent-NDVI area product

The persistent-NDVI method underestimates CRDA-reported palm area by 11–33 %, with the largest discrepancies in Tozeur's earlier years. Because the decoupling analysis operates on anomalies, the constant-fraction bias cancels

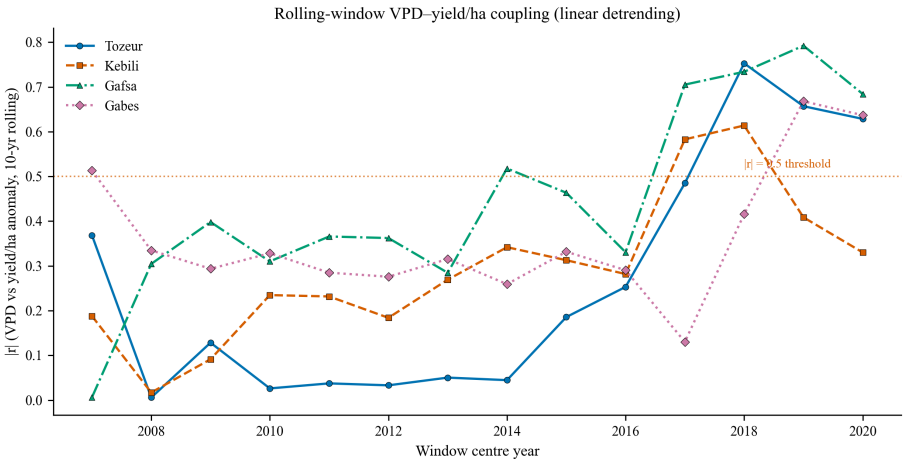

Figure S4: Rolling 10-year absolute correlation between fruit-development-window VPD and linear-detrended yield-per-hectare anomaly for each governorate, with a $|r| = 0.5$ reference threshold. Complements the rolling-slope summary in the main-text Section 4.3.

Table S5: Persistent-NDVI satellite area estimates versus CRDA delegation-level records for years where CRDA data is available. All rows show the satellite estimate as a conservative undercount.

Gov.	Year	Satellite (ha)	CRDA (ha)	Diff. (%)
Tozeur	2021	5,830	8,725	−33.2
Tozeur	2022	6,687	8,725	−23.4
Tozeur	2023	7,781	8,725	−10.8
Kébili	2022	31,738	37,079	−14.4
Kébili	2023	30,927	38,000	−18.6

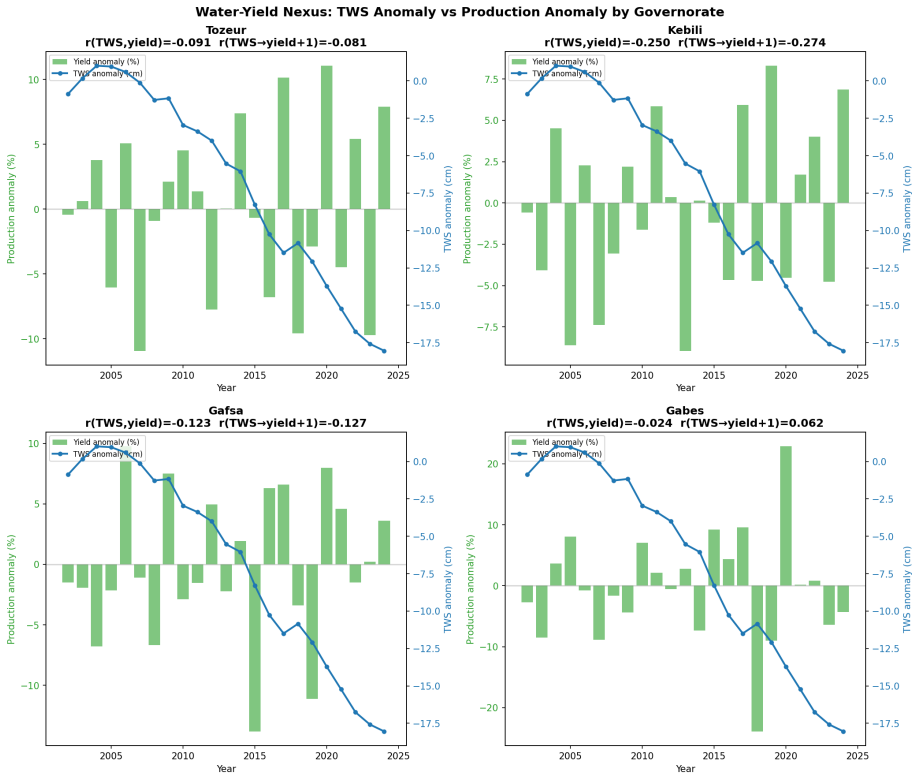

Figure S5: Per-governorate scatter of disaggregated TWS against linear-detrended yield/ha anomaly. The trend is most pronounced in Kébili and Tozeur.

exactly and does not propagate into $\Delta|r|$.

S7. Supervised classification for palm fraction

The palm-fraction correction for Gabès and Gafsa derives from a five-class supervised Random Forest classifier (palm, olive, other irrigated vegetation, bare soil, salt/water) trained on Sentinel-2 surface reflectance (bands B2, B3, B4, B8, B11, B12) and seasonal NDVI statistics. Training labels were photo-interpreted from high-resolution PlanetScope and Google Earth imagery over delegation-level polygons, with a minimum of 30 polygons per class per governorate. A post-classification rule for Gafsa removes non-oasis tree plantations from the palm class using the SRTM-based oasis-depression mask. Overall validation accuracy is approximately 87 % for Gabès (palm-class F1 ≈ 0.91) and 82 % for Gafsa (palm-class F1 ≈ 0.78). The resulting 2024 palm fractions are 0.096 for Gabès and 0.040 for Gafsa; Tozeur and Kébili are assigned palm fraction 1.0 by construction because their Chott-margin continental-oasis footprints contain negligible non-palm dense vegetation, an assumption consistent with the CRDA cross-check (Table S5).

Because the 2024 palm-fraction snapshot cannot be projected backwards across the full record with confidence, the yield-per-hectare decoupling analysis is restricted in the main text to Tozeur and Kébili. For completeness, the corresponding two-period VPD coupling on production anomaly (the only target available at full reliability for Gabès and Gafsa) is shown in Figure S6.

S8. Annual production by governorate

Annual ONAGRI production (tonnes) for the four governorates over 2002–2024 is shown in Figure S7 as a descriptive context plot for the analysis presented in the main text.

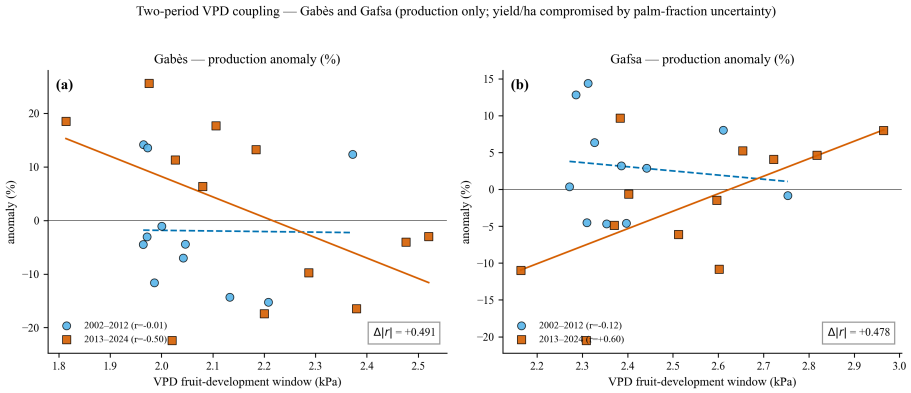

Figure S6: Two-period VPD coupling for Gabès and Gafsa on production anomaly only.

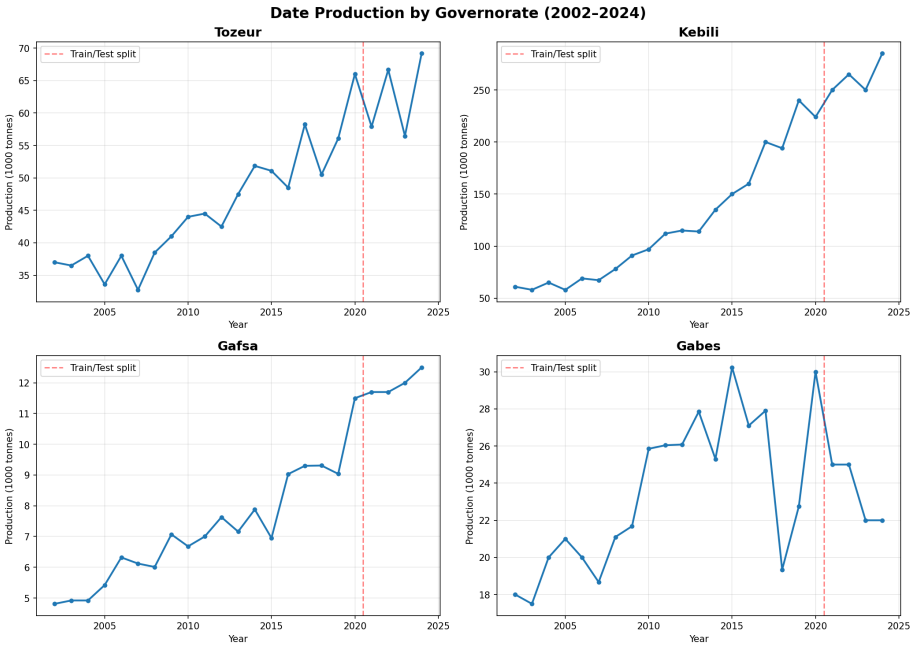

Figure S7: Annual date production by governorate, 2002–2024 (ONAGRI).